AD-A039 345 NAVAL POSTGRADUATE SCHOOL MONTEREY CALIF F/G 13/10

A SCANNING ELECTRON MICROSCOPE STUDY OF THE CORROSION OF SACRIF--ETC(U)

DEC 76 P W WRIGHT

UNCLASSIFIED NL

1 OF 2
ADA
039345

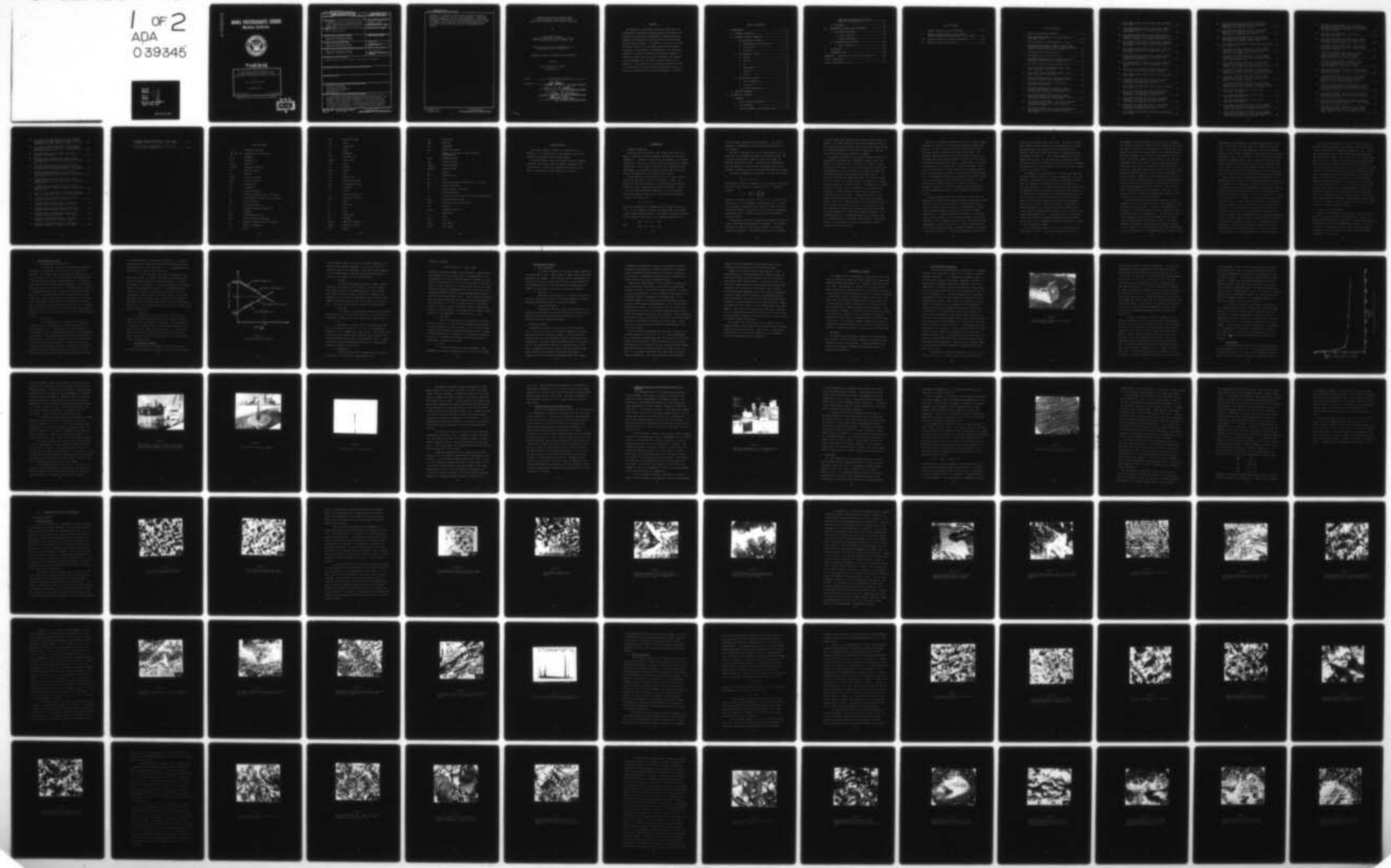

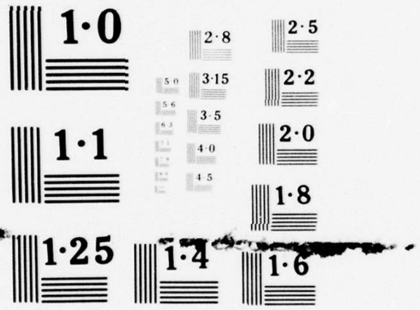

NATIONAL BUREAU OF STANDARDS
MICROCOPY RESOLUTION TEST CHART

NAVAL POSTGRADUATE SCHOOL

Monterey, California

THESIS

A SCANNING ELECTRON MICROSCOPE STUDY
OF THE CORROSION OF SACRIFICIAL HULL
ANODES UNDER SIMULATED SHIP SERVICE CONDITIONS

by

Peter Warren Wright

December 1976

Thesis Advisor: A. J. Perkins

UNCLASSIFIED
SECURITY CLASSIFICATION OF THIS PAGE (When Data Entered)

REPORT DOCUMENTATION PAGE

READ INSTRUCTIONS BEFORE COMPLETING FORM

1. REPORT NUMBER

2. GOVT ACCESSION NO.

3. RECIPIENT'S CATALOG NUMBER

4. TITLE (and Subtitle)
A Scanning Electron Microscope Study of the Corrosion of Sacrificial Hull Anodes under Simulated Ship Service Conditions

5. TYPE OF REPORT & PERIOD COVERED
Master's Thesis;
December 1976

6. PERFORMING ORG. REPORT NUMBER

7. AUTHOR(s)
Peter Warren Wright

8. CONTRACT OR GRANT NUMBER(s)

9. PERFORMING ORGANIZATION NAME AND ADDRESS
Naval Postgraduate School
Monterey, California 93940

10. PROGRAM ELEMENT, PROJECT, TASK AREA & WORK UNIT NUMBERS

11. CONTROLLING OFFICE NAME AND ADDRESS
Naval Postgraduate School
Monterey, California 93940

12. REPORT DATE
December 1976

13. NUMBER OF PAGES

14. MONITORING AGENCY NAME & ADDRESS(if different from Controlling Office)
Naval Postgraduate School
Monterey, California 93940

15. SECURITY CLASS. (of this report)
Unclassified

15a. DECLASSIFICATION/DOWNGRADING SCHEDULE

16. DISTRIBUTION STATEMENT (of this Report)
Approved for public release; distribution unlimited.

17. DISTRIBUTION STATEMENT (of the abstract entered in Block 20, if different from Report)

18. SUPPLEMENTARY NOTES

19. KEY WORDS (Continue on reverse side if necessary and identify by block number)
Sacrificial Anodes
Cathodic Protection
Zinc Corrosion Products
Aluminum Corrosion
Passivation

20. ABSTRACT (Continue on reverse side if necessary and identify by block number)
The behavior of ship hull sacrificial anode zinc was studied under simulated shipboard exposure conditions. The adherence and passivating tendencies of anodic corrosion products are discussed in relation to time and corrosion product layer thickness. The effects of velocity and time of dynamic exposure on zinc anode specimens pre-exposed statically are presented. The behavior of zinc corrosion

products is related to laminar and turbulent regimes of electrolyte flow as well as ionic diffusion. The depassivating tendencies of zinc anode corrosion products are presented. The corrosion of an aluminum sacrificial anode is characterized, and the observed widespread pitting corrosion is hypothesized to be anti-intergranular in nature.

A Scanning Electron Microscope Study of the Corrosion of Sacrificial Hull Anodes under Simulated Ship Service Conditions

by

Peter Warren Wright
Lieutenant Commander, United States Navy
B.S., United States Naval Academy, 1966

Submitted in partial fulfillment of the
requirements for the degree of

MASTER OF SCIENCE IN MECHANICAL ENGINEERING

from the

NAVAL POSTGRADUATE SCHOOL
December 1976

Author Peter W. Wright

Approved by: Jeff Perkins
Thesis Advisor

Terry R. McNelley
Second Reader

Allen E. Fuhs
Chairman, Department of Mechanical Engineering

Robert R. Fossum
Dean of Science and Engineering

ABSTRACT

The behavior of ship hull sacrificial anode zinc was studied under simulated shipboard exposure conditions. The adherence and passivating tendencies of anodic corrosion products are discussed in relation to time and corrosion product layer thickness. The effects of velocity and time of dynamic exposure on zinc anode specimens pre-exposed statically are presented. The behavior of zinc corrosion products is related to laminar and turbulent regimes of electrolyte flow as well as ionic diffusion. The depassivating tendencies of zinc anode corrosion products are presented. The corrosion of an aluminum sacrificial anode is characterized, and the observed widespread pitting corrosion is hypothesized to be anti-intergranular in nature.

TABLE OF CONTENTS

LIST OF TABLES

LIST OF FIGURES

LIST OF SYMBOLS

A A	Arrhenius constant
a_A^a, a_B^b, etc.	elemental ionic activities
Al	aluminum
Al^{+++}	aluminum ion
Al_2O_3	alumina
$Al(OH)_3$	aluminum hydroxide
°C	degrees Celsius
Ca	calcium
$CaCO_3$	calcium carbonate
$CaCl_2$	calcium chloride
Cl^-	chlorine ion
cm	centimeter
cm^2	square centimeter
δ	diffusion boundary layer thickness
δ_o	hydrodynamic boundary layer thickness
D.C.	direct current
E	electrode potential
E^0	standard reference potential
e^-	electron
emf	electromotive force
exp	base of natural logarithms
F	Faraday constant (96,500 coulombs)
°F	degrees Fahrenheit
Fe	iron

fps	feet per second
ft	feet
ft^2	square feet
g	gram
H_2	hydrogen
H^+	hydrogen ion
H_3BO_3	boric acid
H_2O	water
Hg	mercury
hr(s)	hour(s)
in	inch
in^2	square inch
KBr	potassium bromide
KCl	potassium chloride
kg	kilogram
l	liter
ln	natural logarithm
log	logarithm (base 10)
M	metal
M^+	metal ion
$\dot{M}$	mole
m	meter
m^2	square meter
mA	milliamp
$MgCl_2$	magnesium chloride
$MgSO_4$	magnesium sulfate
min	minute

ml	milliliter
mmho	millimho
μm	micrometer
m/s	meters per second
n	number of electrons in cell reaction (Faraday/mole)
NaCl	sodium chloride
NaF	sodium fluoride
$NaHCO_3$	sodium carbonate
Na_2SO_4	sodium sulfate
O_2	oxygen
OH^-	hydroxide ion
Pb	lead
pH	standard hydrogen potential ($pH = -\log a_{H^+}$)
ppm	parts per million
Pr	Prandtl number (diffusion)
Q	activation energy
R	universal gas constant (8.314 joules/degree:mole)
rpm	revolutions per minute
SEM	scanning electron microscope
Si	silicon
$SrCl_2$	strontium chloride
T	temperature
Zn	zinc
Zn^{++}	zinc ion
$ZnSO_4$	zinc sulfate
ZnO	zinc oxide

ACKNOWLEDGEMENT

The author wishes to express his appreciation to Professor A. J. Perkins for his assistance in this work, especially during the final editing stages.

A word of thanks is due Roy Edwards, Material Science Laboratory Technician, for his support throughout this investigation. Chemist Ken Graham also deserves praise for his willingness to help whenever called upon.

I. INTRODUCTION

A. CATHODIC PROTECTION

Corrosion may be defined as the destructive attack of a metal by chemical or electrochemical reaction with its environment [1]. Corrosion in the ocean environment is of extreme importance to the Navy in terms of material failures or reduced capabilities. This work will consider the sacrificial anode performance of a cathodic protection system which is used to protect the underwater hull areas of Naval ships.

Electrochemical corrosion takes place in a cell in which electrical and chemical action is necessary. Such a cell consists of an anode, cathode, electrolyte and some means of external circuit connecting the anode and cathode. In such a cell the anode undergoes oxidation or loss of electrons into the external circuit with a typical metal dissolution reaction; for anodic zinc:

$$Zn \rightarrow Zn^{++} + 2e^-.$$

The resulting positively charged metal ion enters into solution. At the cathode, electrons are gained from the external circuit, and reduction occurs. The cathodic reactions possible in the seawater electrolyte to be considered here are [2]:

$$2H_2O + O_2 + 4e^- \rightarrow 4\,OH^-$$

and

$$2H_2O + 2e^- \rightarrow H_2 + 2\,OH^-$$

with the former equation being predominant. The rate of reduction is dependent on the dissolved oxygen content of the seawater.

One type of galvanic cell is an electrochemical cell in which the two electrodes are made of dissimilar metals, and a natural thermodynamic tendency exists for anodic and cathodic reactions to occur. Current flows spontaneously with the amount of current flowing depending upon the differences in potential existing between the anode and cathode.

The general equation for a galvanic cell can be written as

$$aA + bB \rightarrow cC + dD$$

meaning that a moles of substance A plus b moles of substance B react to form c moles of substance C, etc. The Nernst equation

$$E = E^{\circ} - \frac{RT}{nF} \ln \frac{a_C^c \ a_D^d}{a_A^a \ a_B^b}$$

expresses the exact potential of such a cell in terms of the activities (a) of the products and reactants [1]. Activity is the product of concentration (molality) and an activity coefficient which is a function of the material, temperature and concentration. Tables of activities can be found in corrosion texts.

The galvanic series for seawater lists metals in order of their actual measured potentials in seawater. The relative position of a metal in the series indicates its relative activity or nobility. The more active metal in a galvanic cell will become the anode while the nobler metal becomes the cathode. The anode experiences the electrochemical attack or metal dissolution and positive current (positive current being in a direction opposite to the flow of electrons) flow out into the electrolyte and towards the cathode.

In general, the greater the galvanic series difference in potential of the metals in a bimetallic galvanic cell, the greater the corrosion rate. In addition, cathode to anode area ratio, the extent to which the electrodes are polarized, and properties of the electrolyte will affect the amount of current flowing and the subsequent corrosion rate [1]. In the case of cathode to anode area ratio, for a given current flow in the cell, the current density is greater for a small electrode than for a large electrode. The greater the current density at an anodic area, the greater the corrosion rate; therefore, a large cathode to anode area ratio results in increased anodic dissolution. Polarization refers to the change in electrode potential that takes place as current passes. There are various reasons for this phenomenon which may be found in any corrosion text. Let it suffice to say here that polarization is the difference between the actual electrode potential and the Nernst equation potential. As a cathode polarizes, it becomes more anodic in potential; and as an anode polarizes, it becomes more cathodic in potential. There is a net decrease in total cell potential, and less current flows as a result [3].

The aim of a cathodic protection system is to either supply electrons to the metal to be protected from an external power source or to select a metal more active than the one to be protected and use that metal as a sacrificial anode. The impressed current cathodic protection system has been in use in larger Naval ships and in recent years has been retrofitted into smaller destroyer type vessels. Economically, its initial installation cost is higher than a sacrificial anode system, but its lifetime cost is lower due to the continuing requirement for replacement of anodes in the sacrificial anode system [4]. The impressed current system employs a DC rectifier power source which supplies positive current to an inert or semi-inert auxiliary anode attached to the hull of the ship. An automatic controller is used to maintain the hull potential at some predetermined value to insure complete cathodic protection.

Cathodic protection of ship hulls dates to 1824 when Sir Humphrey Davy reported that copper sheathed wooden hulled ships could be protected from corrosion by employing sacrificial blocks of iron attached to the hull. Unfortunately, cathodically protected copper was subject to fouling by marine organisms [5]. In 1840, Robert Mallet produced a zinc anode that was also suitable. It was not until wooden hulls were replaced by steel, however, that the use of zinc anodes became commonplace on Admiralty vessels [1]. Early cathodic protection systems employed sacrificial anodes primarily in the area of the bronze propeller. The overall cathodic protection of ships was not explored again until 1950. The Royal Canadian Navy showed at that time that the proper application of anti-fouling and anti-corrosion paints in conjunction with a cathodic protection system could result in considerable hull maintenance savings [1]. From a study conducted in 1961 by Francis and Cook [6], it was shown that a projected overall savings of $10,000 to $20,000 in 1961 dollars could be expected per destroyer per 2-year overhaul cycle by utilizing a galvanic cathodic protection system.

The common sacrificial anodes in use today for ship hull galvanic cathodic protection systems are magnesium, zinc, and aluminum. Magnesium is more active or electronegative than zinc or aluminum in the galvanic series in seawater but is only 50% efficient. This means that half the anode deteriorates in seawater without providing any useful protective current. In addition, the high potential of magnesium necessitates the use of dielectric shields between the hull and sacrificial anode, or severe paint damage can occur with a subsequent reduction in overall system effectiveness. Additionally, magnesium anodes are limited to a 2-year replacement cycle while zinc and aluminum anodes may have 3-year, 4-year or even longer replacement cycles. The combination of the aforementioned facts results in magnesium anode systems being more costly than zinc or aluminum and therefore falling into disuse for hull protection systems.

Zinc sacrificial anodes were in use on over 90% of U.S. Naval ships in 1971. In the early stages of zinc anode development, their performance was erratic with a tendency for corrosion products to adhere to the surface and passivate the anode. In 1956, Teel and Anderson [7] reported that the tenacity and electrical resistance of the corrosion product film which formed on the surface of the anode were due primarily to the trace amount of iron present in the zinc and recommended that iron content should be kept below 0.0015%. Subsequent observations by Southin [8] revealed that the addition of aluminum, cadmium and silicon to zinc-iron alloys improved anode performance by alleviating the detrimental effects of iron. Southin [8] also reported that grain size does not affect anode performance. Further investigations by Reichard and Lennox [9] and Waldron and Peterson [10] substantiated and expanded Southin's results. The results of these investigations have been adopted by the Navy in its current MIL-SPEC A-18001H[11] regarding the composition and application of zinc sacrificial anodes.

Aluminum sacrificial anodes have become widely used by commercial ships in recent years due to improvements in their performance and reliability. The initial aluminum alloys developed as sacrificial anodes were very sensitive to heat treatment, grain size and impurities. Two particular high-purity aluminum alloys have proven themselves to be very effective and reliable in hullborne service. The first, Galvalum, developed by the Dow Chemical Company, contains 0.45% zinc and 0.045% mercury and has exhibited efficiencies of 95% in seawater [12]. Although the mercury content of the anode makes it questionable for submarine application, surface ships could readily use this anode in a cathodic protection system. This alloy also has advantages over other aluminum alloys in that no heat treatment is required to insure reliable performance, and its efficiency of 95% is significantly greater than other aluminum anodes. Tests conducted by the Naval Research Laboratory and reported by Lennox [13] noted that some surface areas of the Galvalum anodes remained essentially inactive and in long term use could possibly result in some segments of anodes being lost without producing any useful current.

Another high purity aluminum anode was developed by the Federated Metals Division of the American Smelting and Refining Co. through a U.S. patent held by the Mitsubishi Group [14]. The impetus for this alloy development was provided by aluminum alloy anode users who did not want to use the Galvalum anode because of its mercury content. This alloy contains 4.5% zinc, 0.02% indium and 0.01% cadmium. It has exhibited nominal efficiencies of 85% in service and like Galvalum is not dependent on heat treatment. Its current capacity is 1102 AMP-hr/lb as compared to 1280 AMP-hr/lb for Galvalum and 354 AMP-hr/lb for MIL-SPEC-A-18001H zinc. In tests reported by Haney and Kurr [14] the aluminum-zinc-indium-cadmium alloy exhibited a smoother overall ocrrosion pattern than the striation corrosion pattern of Galvalum as reported by Lennox [13]. Corrosion products formation on these two aluminum alloy anodes has not been investigated in any depth to date and very little exists in the literature on the morphology of these corrosion products.

The virtues of aluminum as a galvanic anode include its relative light-weight and the fact that it can provide over 3 times the current per pound when compared to zinc. Equivalent surface areas of zinc and aluminum have approximately the same current outputs. This means that it is theoretically possible to have a cathodic protection system using aluminum which will weigh the same as zinc but will last 6 years or two typical Naval ship overhaul cycles [4]. The primary reason that the U.S. Navy has not developed a MIL-SPEC for the manufacture and application of aluminum anodes is that the large number of proprietary alloys offered by various producers makes it extremely difficult, if not impossible, to develop a MIL-SPEC around them [15]. This, however, does not prevent the Navy from commercially procuring aluminum sacrificial anodes for installation in Naval ships. The relative metal cost of the aluminum anodes is about two-thirds that of zinc [13], and additional replacement and maintenance savings could be realized through a 6-year replacement cycle vice the current 3-year zinc anode replacement schedule.

B. FACTORS AFFECTING CORROSION

There are a multitude of factors which affect the performance of a galvanic cathodic protection cell. They can be grouped into three general categories: electrochemical aspects, environmental effects and metallurgical aspects. The most relevant of the factors in each of these categories shall be discussed in order to present a basis for possible further discussion in this thesis.

1. Electrochemical Aspects

a. Thermodynamic Considerations

In order for a reaction to proceed spontaneously, there must be a reduction in the total free energy of the reactants. The Nernst equation expresses the potential of a cell in terms of the activities of products and reactants and is derived from free energy considerations [1]. A positive Nernst equation total cell potential indicates that oxidation of a metal in that cell will occur. The rate of cell corrosion is determined by other factors that will be discussed separately [1]. The larger the potential difference of the electrodes in a galvanic corrosion cell, the greater the corrosion rate, other factors affecting corrosion rate not considered. Thus the relative position of electrode materials in a galvanic series indicates the direction of probable cell reaction and relative corrosion rate in the absence of other rate-influencing factors.

b. Polarization

This phenomenon can be thought of as retarding corrosion rate by decreasing the corrosion current of an electrochemical cell. Polarization is usually divided into two different types: activation polarization and concentration polarization. Activation polarization refers to an electrochemical process which is controlled by the reaction sequence at the metal-electrolyte interface. Every reaction has a finite activation energy required to proceed, and activation polarization can be thought of as the slowing of the total electrode reaction because of an activation energy that must be attained before the reaction can proceed [1]. Concentration polarization occurs for electrochemical reactions which are controlled by ionic diffusion, i.e., are dependent on the availability of ions in the electrolyte.

As stated earlier, when an electrode acting as a cathode polarizes, it becomes more anodic in potential; and when an electrode acting as an anode polarizes, it becomes more cathodic in potential. A simplified general polarization diagram is represented in Figure 1. As polarization rates increase, the slopes of the polarization curves increase resulting in a lower value of corrosion current (i_{corr}) and subsequent lower corrosion rate. Generally, for a galvanic corrosion cell, activation polarization occurs for both anode and cathode, while concentration polarization only affects the cathodic reaction [3].

c. Passivity

Essentially, passivity refers to the loss of chemical reactivity experienced by certain metals and alloys under particular environmental conditions. This phenomenon is difficult to define because of its complex nature and the specific conditions under which it occurs [3]. For the purposes of this thesis, passivity will refer to the loss of anodic reactivity due to the buildup of a thick and adherent corrosion product film.

2. Environmental Effects

Since seawater is a complex solution of many salts containing living matter, suspended silt, and dissolved gases,

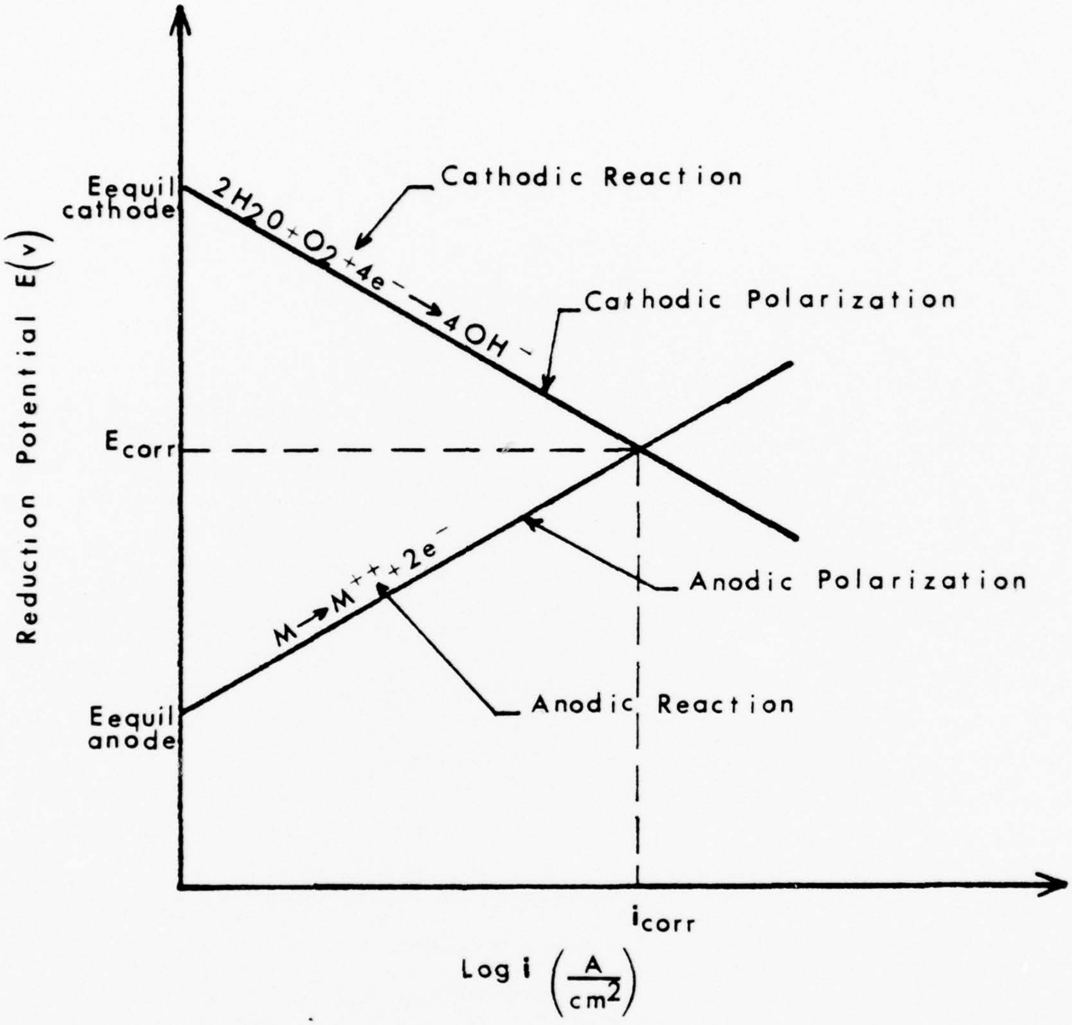

Figure 1

General polarization diagram

the individual effect of each of the factors affecting corrosion is not readily separable. The use of artificial seawater in this work eliminates living matter and suspended silt considerations so that only the factors affecting corrosion in this thesis will be discussed here.

a. Oxygen

The dissolved oxygen content is a major factor affecting the corrosivity of seawater. For most galvanic reactions in seawater, the depolarization of the cathode is more rapid with the increase in arrival of oxygen at the cathode, which in turn is a function of the dissolved oxygen content of seawater and the velocity of flow at the surface [16]. Generally surface water is high in oxygen content.

b. Salinity

The salinity of open ocean surface waters typically range from 32 to 37.7 parts per thousand. In this range the corrosion of common metals is not appreciably affected [16].

c. pH

Seawater is slightly basic with pH varying from 8.0 to 8.3 near the surface to 7.7 to 7.8 at intermediate depths to 7.0 in stagnant deep ocean basins. High pH and high dissolved oxygen content, and conversely low pH and low dissolved oxygen content, usually occur together [16]. As experimental pH values were controlled, pH was not a significant corrosion variable in this work.

d. Temperature

Usually an increase in temperature will increase the severity of corrosion as represented by the

Arrhenius equation.

$$\text{rate of corrosion} = A_{\exp}(-\,B/_{RT})$$

where all the symbols except T are constants. Recent work by Mor and Beccaria [17] on the effect of temperature on the corrodibility of zinc in aerated synthetic seawater at zero velocity indicates this is the fact for periods of time up to about 72 hours. However, the reverse trend occurs for long immersion periods at temperatures of 40°C to 60°C due to the increasing precipitation of calcium and magnesium carbonate onto the initial passivation layer. These additional products make the passivation layer more compact and less permeable to the diffusion of Zn^{++} ions resulting from the dissolution reaction. Ships typically experience seawater temperatures in the 0°C to 30°C range. The conductivity of seawater nearly doubles as the temperature is raised from 0° to 25°C.

e. Velocity

Most corrosion products which form on a surface inhibit corrosion. If they are soft, currents may wash them away and increase the corrosion rate. Also, if the cathodic reaction is controlled by concentration polarization, removal of the concentration by currents will increase the corrosion rate [16]. The effects of velocity on corrosion product morphology is a part of this work.

f. Time

All corrosion rates are time dependent. Time dependency in various situations will be a part of this work.

3. Metallurgical Aspects

a. Grain Boundaries

As a metal solidifies, the atoms arrange themselves in a crystalline array. These arrays or grains meet, and grain boundaries are formed. Since the most stable configuration of the metal is its particular crystal lattice, grain boundaries are high-energy areas. They are more active chemically and usually are attacked more rapidly by a corrosive medium.

b. Alloying

From previous discussion it is evident that alloying has a significant effect on the passivating film forming properties and efficiencies of sacrificial anodes.

c. Surface Conditions

Inclusions, scratches, other surface defects, or elemental distribution may provide initiation sites for microanodic or microcathodic regions and significantly affect corrosion and film formation processes.

C. PREVIOUS RESEARCH

Significant research was carried out from the middle 1950's to the late 1960's concerning development of reliable and efficient zinc sacrificial anodes. This research was mentioned earlier in the cathodic protection section of this introduction. The period from the middle 1960's to the present has seen additional research, including studies in the area of aluminum sacrificial anodes, the two previously mentioned alloys being the most significant developments. Recently, work at the Naval Postgraduate School has sought to examine the morphology of anodic zinc corrosion products through the application of surface microanalytic techniques such as scanning electron microscopy and energy dispersive X-ray analysis. Pertinent conclusions follow regarding the recent works at the Naval Postgraduate School.

Despite the improvements in zinc sacrificial anodes previously mentioned, instances of passivation of anodes have continued to occur, even when the material adheres to compositional specifications. In 1973, Bornholdt and Perkins [18] initiated studies to characterize the morphology of zinc corrosion products via scanning electron microscopy in order to gain a better general understanding of zinc corrosion and passivation problems. They discovered that the typical corrosion product consisted of dense but microscopically porous arrays of hexagonal zinc oxide (ZnO) platelets. These platelets form with the basal planes of the ZnO crystal structure oriented parallel to the broad, slow-growing external faces. These plates also tend to be oriented nearly perpendicular to the zinc alloy surface.

Todd and Perkins continued investigations of anodic zinc corrosion products in 1974 [19, 20, 21]. They concentrated on the nucleation and growth process of the type of corrosion product described above. They postulated that a thin supersaturated layer of dissolved zinc ions above the metal surface made possible the observed nucleation of single crystals of ZnO. It was further postulated that under long term static exposure conditions, zinc oxide platelets would eventually begin to grow more parallel to the metal surface, thus producing a passivating film of corrosion products.

Luebke [22] continued these investigations in 1976, concentrating on zinc corrosion product behavior under conditions of varying relative velocity with the electrolyte and varying anode current density. In order to carry out this work, Luebke designed and constructed an exposure tank assembly with a rotating disk electrode, with a voltage-controlled current generator device that allowed independent control of anode relative velocity and impressed current. After developing a data base of zinc anode corrosion product behavior at various velocities and current densities, Luebke concluded that passivation of a zinc anode under low current density, long time, static exposures was possible. Additionally, he concluded that anode passivation did not take place in high velocity turbulent conditions, due to a cyclic process of product buildup and spalling.

The present work concentrated on zinc anode corrosion product behavior under conditions which more closely simulate shipboard exposure conditions. Additionally, an exploratory investigation into the corrosion behavior of an aluminum sacrificial anode material was conducted.

II. EXPERIMENTAL PROCESS

The purpose of the experimental process used in this work was to simulate the conditions that a sacrificial anode would experience while hullborne in the cathodic protection system of a ship. As mentioned in the previous section, work to date at the Naval Postgraduate School has utilized zinc sacrificial anodes in static conditions only or in dynamic conditions in which both velocity and current density were varied. The life cycle of a typical hullmounted sacrificial anode would include periods of static conditions while the ship was in port and periods of dynamic conditions while underway. This work sought to simulate a situation in which sacrificial anodes were allowed to corrode in static conditions for varying lengths of time followed by underway periods of varying velocity and time. The corrosion product morphology was studied throughout this experimental process in order to establish the behavior of sacrificial anodes in a more real-life experience.

A. APPARATUS

The apparatus used included a beaker in which specimens were exposed to static seawater conditions, cylindrical tank container, rotating disk assembly, current generator/power source, and a digital voltmeter and frequency counter as monitoring instruments.

1. Static Exposure Apparatus

The static exposure apparatus consisted of a standard, 3000 ml, pyrex laboratory beaker which contained a synthetic seawater electrolyte. This apparatus is somewhat similar to the one Todd [21] used in his work. Appendix A contains the specification standards followed and chemicals used in its preparation. Synthetic seawater specifications require that its pH values range from 8.0 to 8.4 and conductivity from 39.0 to 45.0 millimhos [23]. Before and during static exposures the conductivity and pH were checked and maintained within the prescribed values. Usually only the addition of a small amount of distilled water, to compensate for evaporation losses, was necessary to maintain the seawater electrolyte as prescribed. The specimen was galvanically coupled to a steel plate and mounted on a plexiglass stand by means of a nylon bolt which passed through a hole in the stand and a hole in the steel plate and threaded into a tapped hole in the back of the specimen as shown in Figure 2. The specimen stand was then placed in the beaker in a near-vertical position in order to more closely simulate the orientation of a sacrificial anode on a ship's hull. The cathode to anode area ratio utilized would greatly affect the anodic galvanic current density experienced by the specimen. Therefore, great care was taken to insure that an exact, reproducible cathode-to-anode area ratio was utilized.

The sacrificial anode was machined to 7/16 in x 7/16 in x 3/16 in (1.1 cm x 1.11 cm x 0.48 cm) in order to fit the

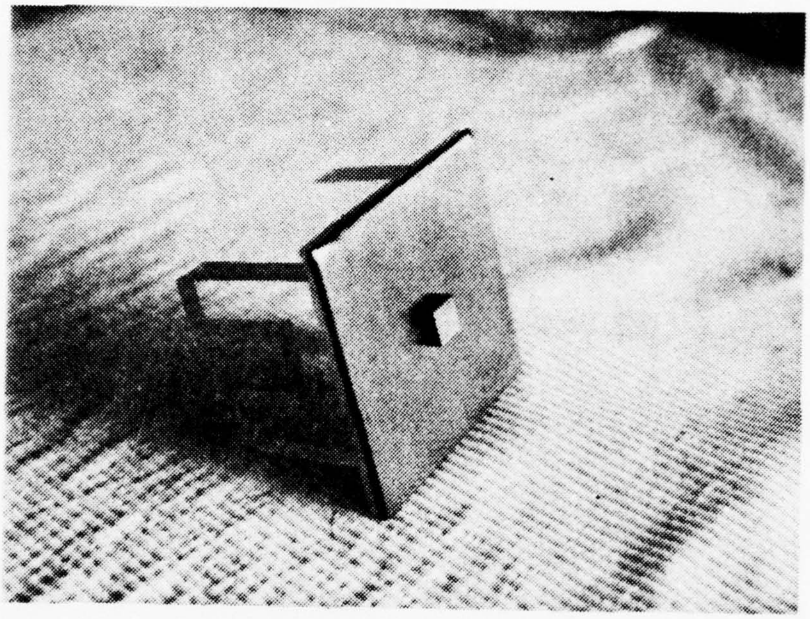

Figure 2

Anode specimen coupled to a steel plate on a plexiglass stand rotating disk assembly to be discussed later. The sides of the anode were spray painted with black insulating dope so that galvanic current would only pass through the 7/16 in x 7/16 in faces of the anode. Additionally, the sides and back of the 3 in x 3 in x 1/8 in (7.62 cm x 7.62 cm x 0.32 cm) steel plate were also sprayed with black insulating dope so that only the bare 3 in x 3 in face would act as a cathode. The anode specimen then coupled to the steel cathode produced an area ratio of 46 to 1. This area ratio closely conforms to Military Specification A-18001H requirements for the cathodic protection of bare steel with military specification zinc sacrificial anodes. Additionally, the painting of the sides of the anodes helped to reduce complicated corrosion edge effects due to nonuniform galvanic currents through the specimen [24].

In order to determine a value of galvanic current density experienced by the sacrificial anode, a measurement was made of the total cell galvanic current. The measurement system simply consisted of a sacrificial anode electrically connected to one side of a Weston model 1240 digital multimeter by a glass insulated support rod and low resistance wire and a steel plate connected to the other side of the multimeter by an insulated support rod and low resistance wire. Both the specimen anode and steel plate were painted with insulating dope to insure a 46 to 1 cathode to anode area ratio. The anode and cathode were suspended in a 3000 ml beaker of synthetic seawater electrolyte in close proximity to one another, the bare face of the anode facing the bare face of the steel plate. The current passing through the cell was monitored, and a plot of this current versus time is shown in Figure 3. The galvanic current measured in this manner is slightly less than that experienced by a direct contact galvanic couple due to the resistivity of the electrolyte between anode and cathode. The value obtained, however, serves as an approximate value and is considered accurate enough for this experimental process. To measure more accurately the galvanic current, a zero impedance ammeter as described by Champion [25] would be suitable.

The value of galvanic current density determined in this manner is about 5 mA/in^2 (0.775 mA/cm^2) for a zinc/steel couple. This value of current density differed from that of 10 mA/cm^2 (1.55 mA/cm^2) determined by Luebke [22] as an approximation to the current density experienced by Todd [20] in his work with 50 to 1 cathode to anode ratio zinc/steel couples. This difference could be attributed to differences in cell geometry or in methods of determination. However, the values are of the same order of magnitude, and it was felt that future correlation differences would not be significant.

2. Tank Assembly

The tank assembly used in this work was designed and used by Luebke [22] in his work. It was constructed entirely of plexiglass and was 18 in (45.72 cm) in diameter and held about 13 gal (49 liters) of synthetic seawater electrolyte.

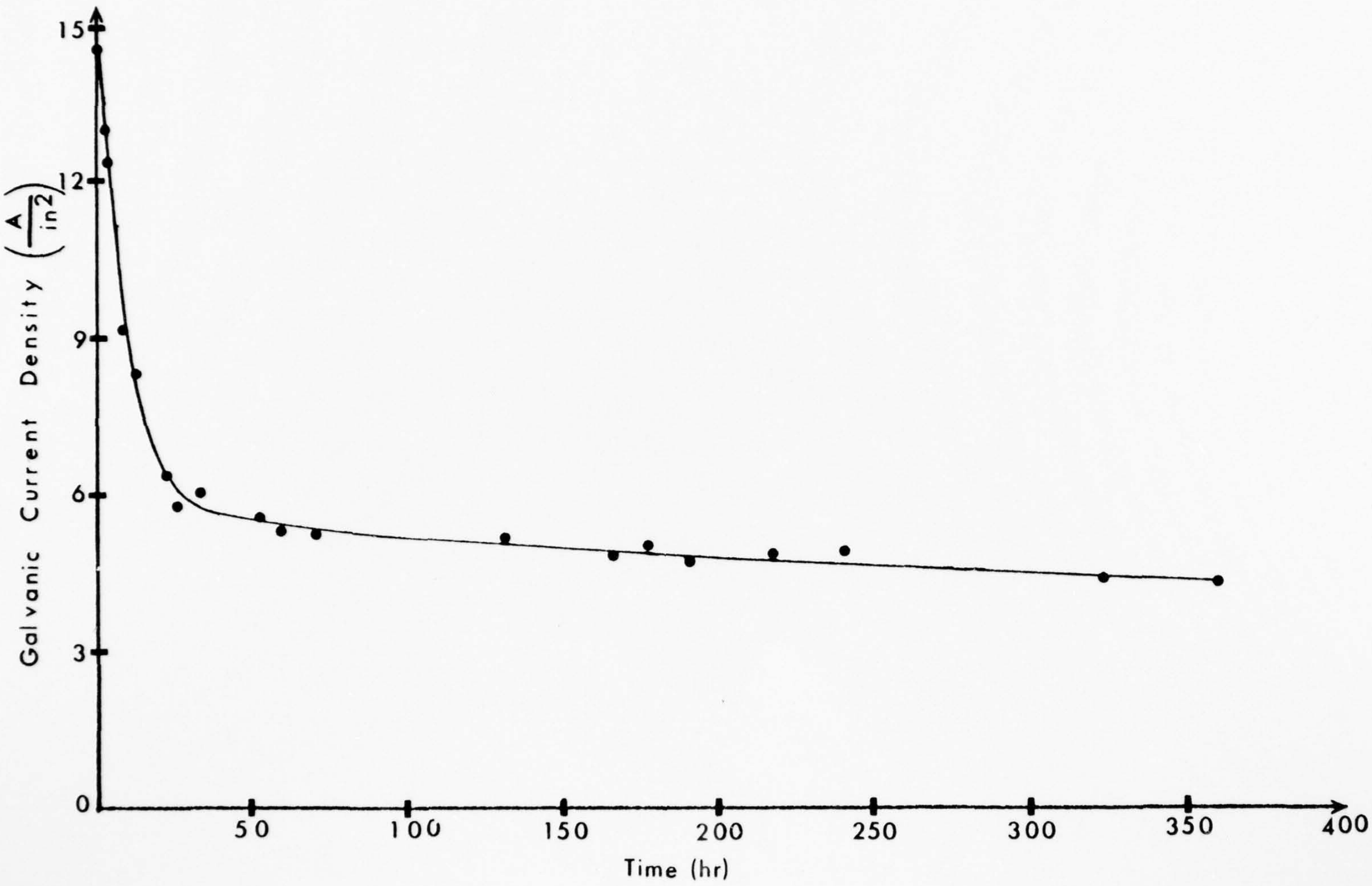

Figure 3

Plot of galvanic current density vs. time

A system of baffle strips was installed in order to keep the electrolyte as stationary as possible during traveling electrode experiments. The relatively motionless fluid/traveling electrode situation created by this arrangement was somewhat similar to that experienced by shipboard zincs. An aeration canal was fitted into the bottom of the tank which allowed compressed air to be bubbled through the liquid from an array of 12 equally spaced air holes. An attached regulator and air filter insured a precise flow of clean air into the electrolyte. Figure 4 shows the tank construction.

A rotating disk electrode was used to expose the anode samples to velocity effects. It consisted of a 12 inch (30.48 cm) diameter; 1/2 in (1.27 cm) thick plexiglass disk suspended by a 1 in (2.54 cm) diameter plexiglass shaft. The shaft was connected via a pulley arrangement to an electric motor. Variations in pulley size allowed disk speed to be varied from 6 to 210 rpm. Figure 5 illustrates the assembly.

Each anode specimen was located in the disk underside in a small rectangular slot near the outer perimeter of the disk as shown in Figure 6. The distance from the center of the disk to the center of each sample was 5.70 inches (14.48 cm). The slot was machined so that the specimen fitted with minimum tolerance and was flush with the disk surface. Minimum solution disturbance was realized with this scheme.

The specimen was held in the slot by a plastic screw threaded into the tapped hole in the back of the specimen. The screw entered the disk from its top surface; and when in place, the top of its head was flush with the surface.

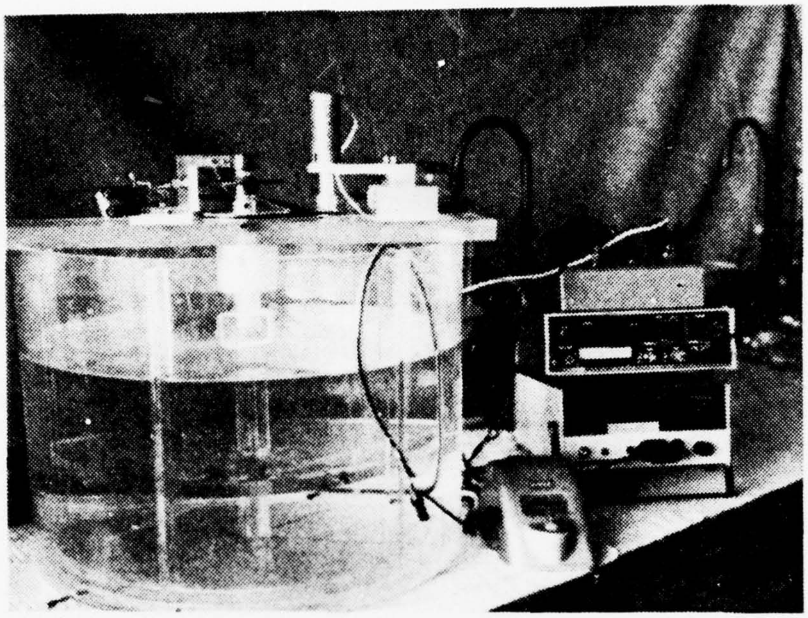

Figure 4

Experimental apparatus showing exposure tank, rotating disk assembly, timer, current generator, digital counter, and digital voltmeter

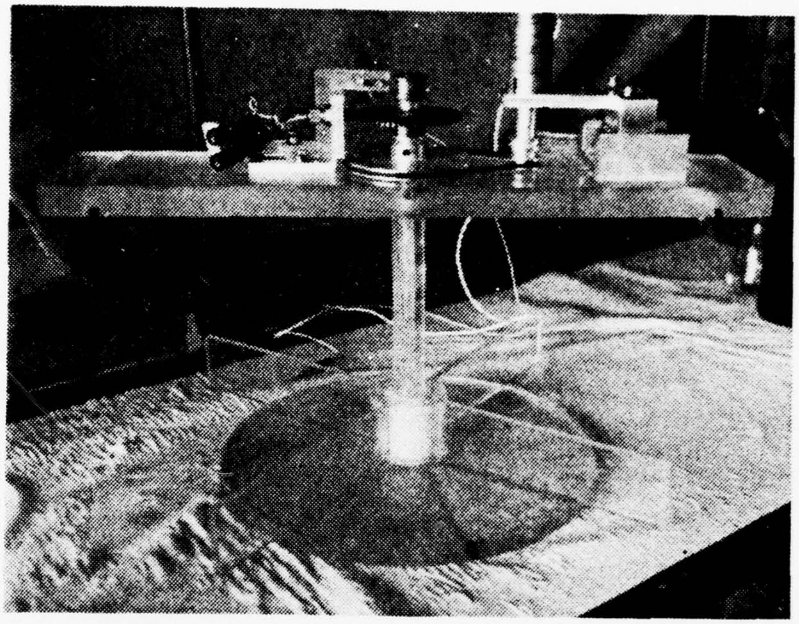

Figure 5

Rotating disk electrode assembly

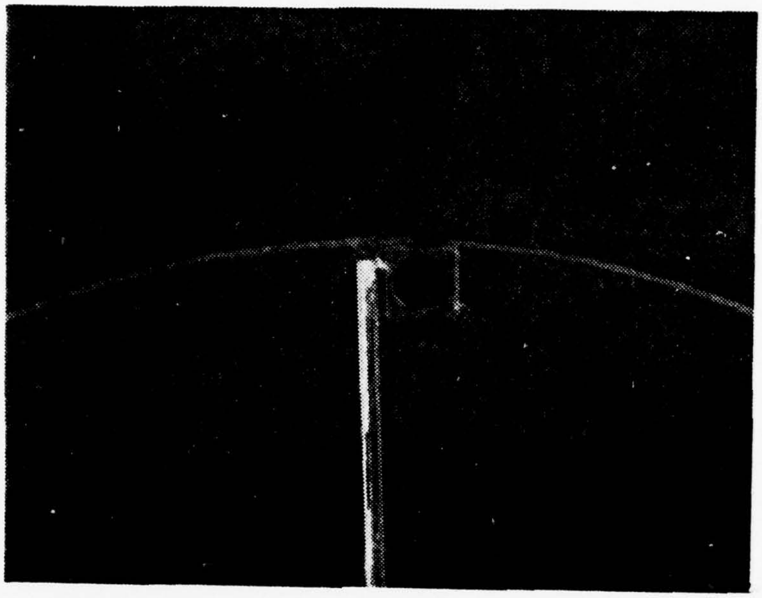

Figure 6

Rectangular slot in rotating disk

The impressed galvanic current was supplied to the anode through a brass ring, located in the slot, which made contact with the specimen. Current was supplied to the brass ring by a copper wire placed within a hole drilled along the disk radius to its center. At this point the wire passed into the hollow connecting drive shaft and then up out of the tank and connected to a brass ring at the top of the drive shaft. A copper brush rested against the brass ring. Connection from the current source to the brush allowed the anode specimen current to be controlled regardless of its velocity. In this arrangement current was delivered to the anode specimen via a watertight route to guarantee that only the specimen would corrode.

The top of the shaft was fitted with a 60 tooth gear in addition to the brass ring. A magnetic pickup, positioned near the gear and attached to the digital frequency counter, sensed a magnetic flux as each geartooth passed during operation. These flux signals were instantaneously converted into rpm and displayed by the counter.

A platinum impressed current cathode was utilized because of its non-fouling characteristics regarding the electrolyte. This electrode assembly consisted of a thin 1.50 in (3.81 cm) diameter platinum disk that was positioned to rest on top of the bottom baffles and at the center of the tank, approximately 1.25 in (3.18 cm) below the plexiglass disk. As the disk assembly rotated, the distance from the platinum cathode to the anode specimen remained a constant 5.84 in

(14.82 cm). The platinum disk was welded to a platinum wire which passed immediately into a sealed piece of glass tubing connected to a current source lead which passed through sealed plastic tubing and out of the tank. Thus the platinum disk was ultimately connected to the current source via a watertight route.

3. Current Generator and Voltage Source

This piece of apparatus was designed by Mr. Tom Christian of the Department of Mechanical Engineering and was also utilized by Luebke [22]. The device was capable of supplying the current necessary for the corrosion as well as that required by the electric D.C. motor to rotate the plexiglass disk. Equipped with separate voltage and current generators, it could perform both functions simultaneously or singly. It was possible to control anode specimen current to ± 2 microamps and disk rotation to ± 1 rpm. Current output from the voltage controlled current generator was governed by the selection of a particular voltage across one of four precision resistors, and this voltage was monitored with the digital voltmeter. The chosen resistor was automatically placed in series with the load (anode) so that the current through the load was identical to that through the resistor. Maximum current available was 0.75 amps (7.50 volts with a 10 ohm resistor). A more comprehensive description of the tank assembly, rotating disk electrode and voltage/current generator may be found in Luebke's [22] work.

4. Scanning Electron Microscope and PGT 1000 X-ray Analyzer

The Cambridge model S4-10 Stereoscan Scanning Electron Microscope (SEM), shown in Figure 7, was utilized to study the surface morphology of each anode specimen. The SEM enjoys a considerable advantage over the conventional light microscope in terms of depth of focus and useful magnification. The SEM depth of focus is about 300 times greater than a light microscope at equivalent magnifications, and the useful magnification is about 10,000X. For the purposes of this study, magnifications of up to 5000X were utilized. The SEM also provides an operator with the ability to translate a specimen in the x, y, and z directions, rotate 360°, and tilt from 0° to 90°.

The SEM focuses a beam of electrons on a sample surface by means of electromagnetic lenses. Bombardment of the surface results in the emission of secondary electrons, as well as backscattered electrons, X-rays, and Auger electrons. The secondary electrons emitted are detected in an electron collection system which consists of a scintillator, a photomultiplier, and several amplifiers which ultimately deliver the signal to the cathode ray tube for display. The cathode ray tube beams are synchronized with the electron gun scan of the SEM. The ratio of the length of a scan line on the cathode ray tube to the length of a scan line on the specimen is the magnification of the image seen.

As the secondary electrons are emitted at various angles from the surface of the specimen, the picture developed

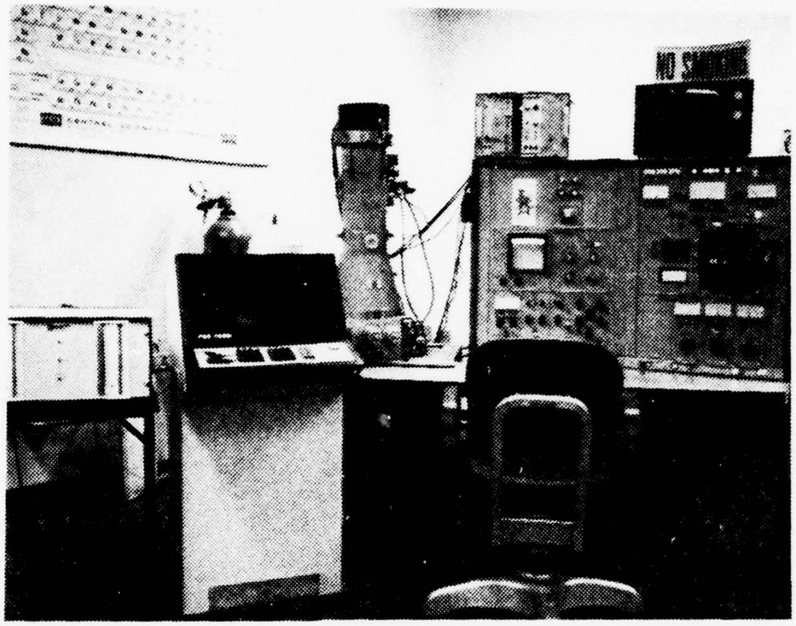

Figure 7

Cambridge Stereoscan S4-10 scanning electron microscope and PGT 1000 X-ray analyzer is three dimensional in appearance and differs very little from the actual specimen surface. Light and dark areas on a SEM display indicate variations in topography as well as conductivity of the surface. More conductive areas appear darker due to fewer secondary electron emissions. The ability to discern different areas of surface conductivity is particularly valuable in corrosion research.

Coupled to the Naval Postgraduate School SEM is a Princeton Gamma Tech 1000 energy-dispersive X-ray analyzer. The analyzer detects X-rays emitted from the specimen surface by the use of a solid state Si(Li) semiconductor detector located in the SEM specimen chamber. The analyzer processes the detector signals to display an energy spectrum. Direct identification of elements is possible from the characteristic X-ray energies present. The analyzer displays a spectrum of energy levels in which relatively large peaks indicate relatively large amounts of specific elements. This elemental analysis can be extremely useful in identifying trace elements found in anode alloys or elements found in corrosion products.

B. PROCEDURE

The zinc samples used in experimentation were cut from a hull sacrificial anode conforming closely to Military Specification A-18001H [11] zinc. A comparison of spectrographic analysis of this zinc alloy with MIL-SPEC zinc is made in Tables I and II. The aluminum samples used were cut from an aluminum hull sacrificial anode conforming closely to the specifications of Galvalum and provided by the Naval Research

Laboratory, Washington, D.C. A spectrographic analysis of this alloy is found in Table III.

Prior to exposure, the surface of each specimen was ground on 3-0 emery paper, rinsed in ethanol and distilled water and air dried. This was done to minimize the effects of surface roughness and cleanliness on the reproducibility of data. Figure 8 shows a typical surface, ready to be used in an experiment. Prior to each experimental run, the conductivity and pH of the seawater electrolyte were tested to insure that they were within prescribed limits [23].

The specimens were coupled to the steel plate and plexiglass stand by the nylon bolt. The steel surface was previously ground and free of rust deposits. The stand assembly was placed in a near vertical orientation in the static beakers for varying periods of time up to 8 days. The aluminum anodes were only exposed for periods of up to 2 days as it was found that the pH of the beaker solution could not be maintained properly. The exact cause of this problem was not ascertained. It is conjectured that a probable hydrolysis reaction of the type described by Galvele [26]

$$Al^{+++} + 3H_2O \rightarrow Al(OH)_3 + 3H^+$$

was taking place, and the subsequent high concentration of H^+ ions was causing the electrolyte pH to decrease. An attempt to control the electrolyte pH by aeration was not successful, and it was decided to limit the exposure of aluminum anodes to 2 days duration. The investigation of aluminum sacrificial

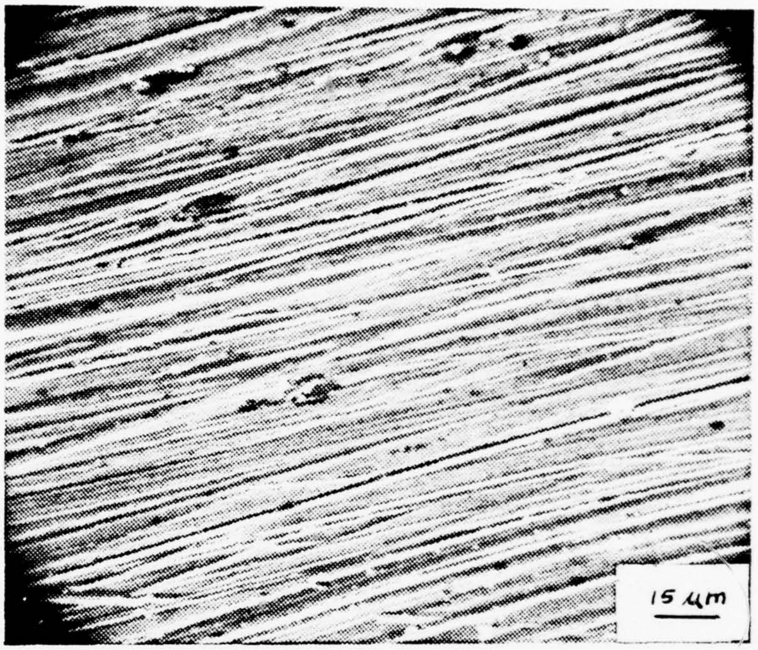

Figure 8

Polished surface of anode specimen, 640X anode behavior is only exploratory in this work. The principal aim is the further investigation of zinc anode morphology.

Zinc specimens were corroded in three different beakers for the same time period. Thus it was possible to examine all three specimens via the SEM to insure uniformity of corrosion product morphology prior to further testing. Aluminum specimens were corroded singly. Upon removal of the anode specimens from the static beakers, they were gently rinsed in distilled water, air dried, and mounted on a special threaded SEM stub which allowed the subsequent removal and retesting of the specimens in further experiments. The specimens were then characterized for surface corrosion product morphology by SEM examination and subsequent photographing. These photomicrographs provided the initial basis of information to which further corrosion product behavior would be related.

Following their static corrosion characterization, the specimens were fastened into the rotating disk electrode slot. Impressed corrosion current checks were made to insure that current applied would be that actually prescribed by the experimental plan. The current density used for the bulk of this work was the 5 mA/in^2 (0.775 mA/cm^2) galvanic current density whose determination was described earlier. There were a few departures from this value to higher values for experimental comparisons.

The rotating disk assembly was then lowered into the electrolyte and the rotating disk brought up to prescribed rpm. Once the desired rpm was reached, the corrosion current was applied to the anode, and an electric timer started.

Upon completion of the testing period, the corrosion current was turned off and the rotating disk assembly removed immediately. The insertion and removal of the rotating disk assembly and the start and stop of the current and voltage generator was done as quickly as possible to minimize any local corrosion of the anode. The speeds of the rotating disk assembly utilized were primarily 50, 100, 150, and 200 rpm. The fluid dynamics of rotating disk electrodes are well known, and the actual resultant velocity vector experienced by the anode specimen is a function of rpm, disk radius, and bulk fluid disturbances [27]. The exact velocities experienced are in themselves not as significant as relative velocities for the purposes of this work. However, the question of laminar or turbulent flow is particularly significant in terms of boundary layer behavior of corrosion products. A. C. Riddiford [28] reports that the transition from laminar to turbulent boundary layer conditions begins at Reynolds numbers of about 2×10^5 and transition is complete at a Reynolds number of 3×10^5 for a rotating disk electrode. For the experimental rpms utilized in this work, the following Reynolds numbers apply:

RPM	Re
50	1.05×10^5
100	2.09×10^5
150	3.14×10^5
200	4.19×10^5

Therefore, the anode specimens experienced laminar as well as turbulent boundary layer conditions. Luebke [22] conjectured that turbulent boundary layer conditions existed at speeds of rotation of 100 rpm and greater which correlates reasonably well with the data presented here. The specimen was removed from the slot and immediately rinsed with a gentle stream of distilled water, so as not to disturb the corrosion products, and air dried. The specimen was then remounted on the threaded SEM stub and subjected to further SEM characterization.

A designation system shall be utilized to identify specimens. The first number indicates the length of time of static exposure followed by the units of exposure time, hours (H), or days (D). Then a letter Z for zinc or A for aluminum will be followed by a number designating the specimen within the indicated static exposure group. For example, 36HZ1 indicates zinc specimen number 1 within the 36 hour static exposure group. A compilation of specimen exposures appears in Table IV.

III. EXPERIMENTAL RESULTS AND DISCUSSION

A. ZINC ANODE SPECIMENS

1. Static Exposures

In order to establish a reproducible corrosion product condition prior to dynamic exposures, three specimens were subjected to identical static environmental conditions. This procedure established that the corrosion product morphology of statically exposed sets of specimens was nearly identical, as evidenced by Figures 9 and 10 which show two different specimens after 2 hours exposure each. For periods of static exposures over 12 hours, somewhat greater variations existed in corrosion product morphology. However, these variations were minor in degree and were easily characterized and compared, so that the static exposure data base remained reliable. These variations may have been due to slight differences in static exposure electrolyte pH or conductivity or slight differences in specimen surface preparation.

The static corrosion products seen in this work were nearly identical to those reported by Todd [20], except that there seemed to be an increased rate of corrosion product growth in this work, especially in early growth stages. The effect of painting the sides of the sacrificial anode specimen is thought to be the cause of this accelerated growth. With the sides painted, the edge-to-area ratio was decreased, and a very uniform dissolution was noted across the specimen surface.

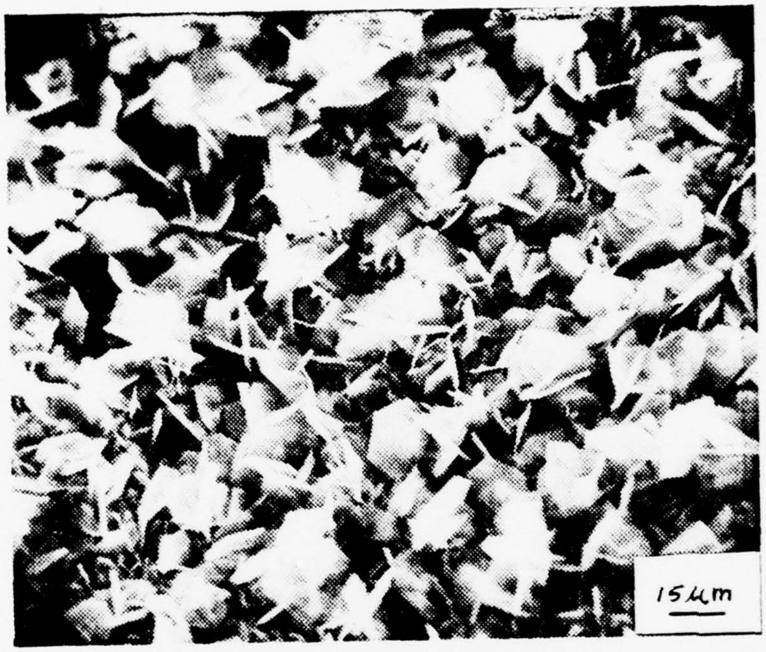

Figure 9

Zinc anode surface appearance after
2 hour static exposure, 540X (2HZ1)

Figure 10

Zinc anode surface appearance after 2 hour static exposure, 540X (2HZ3)

Figure 11 exhibits this uniform dissolution and indicates that a very uniform galvanic current density was evident across the surface due to the reduction of corrosion edge effects and the elimination of current passing through the sides of the specimen.

Todd [21] postulated that the development of a passivating layer was possible during static exposure conditions. He observed what he thought to be a passivating film after one week exposure. This passivating film was characterized by ZnO platelets growing parallel to the anode surface and seemingly to coalesce. In this work, no such platelet growth was observed. Instead, the morphology of this work remained as ZnO platelets growing individually and in clusters up to the maximum static exposure of 8 days. Figure 12 is an example of corrosion product growth after 4 days of static exposure.

It was found that corrosion products exhibited periods of less adherence to the anode surface and actually washed off during the gentle rinsing following a static exposure. Figures 13 and 14 are micrographs of a 24 hour static exposure specimen. The two layers of corrosion product evident in Figure 13 are the result of the outer layer loosening during static exposure, exposing the underlying zinc surface and permitting subsequent nucleation and growth of ZnO platelets on the surface. In Figure 14, the extension of the underlying platelet layer under the outer platelet layer can be seen for a small distance.

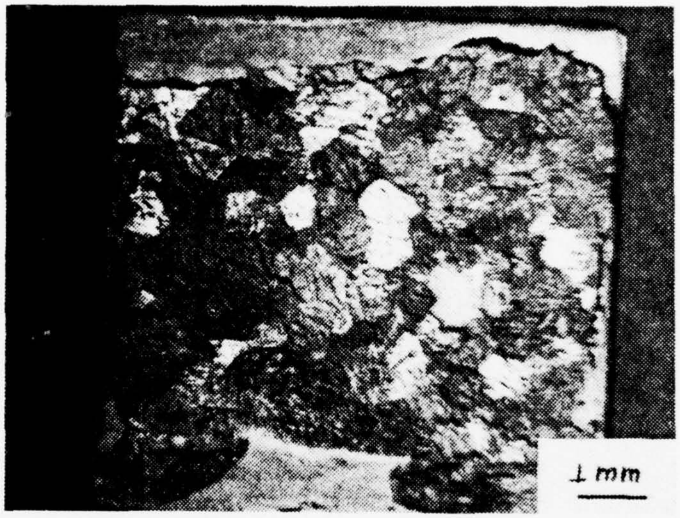

Figure 11

Zinc anode surface after corrosion products removed showing uniform dissolution, 10X

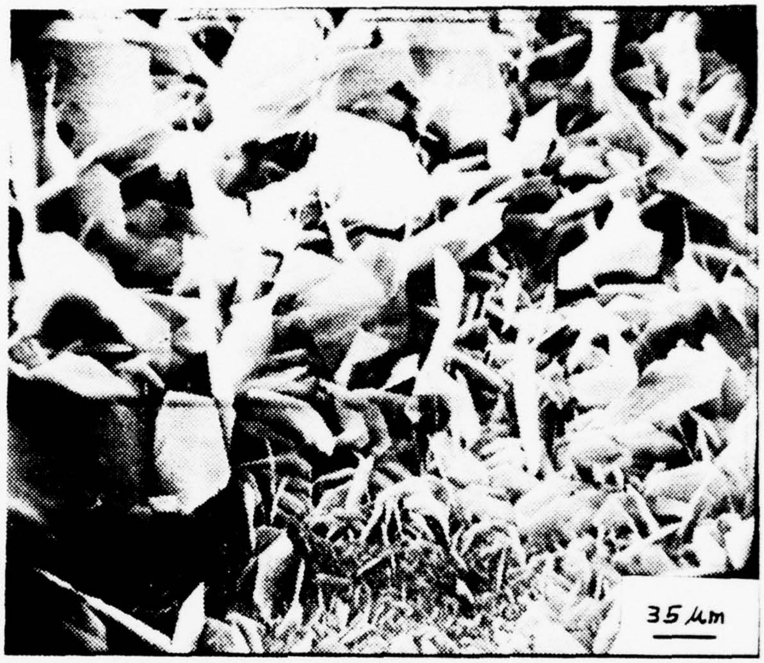

Figure 12

Zinc anode surface after 4 days static exposure, 260X (4DZ3)

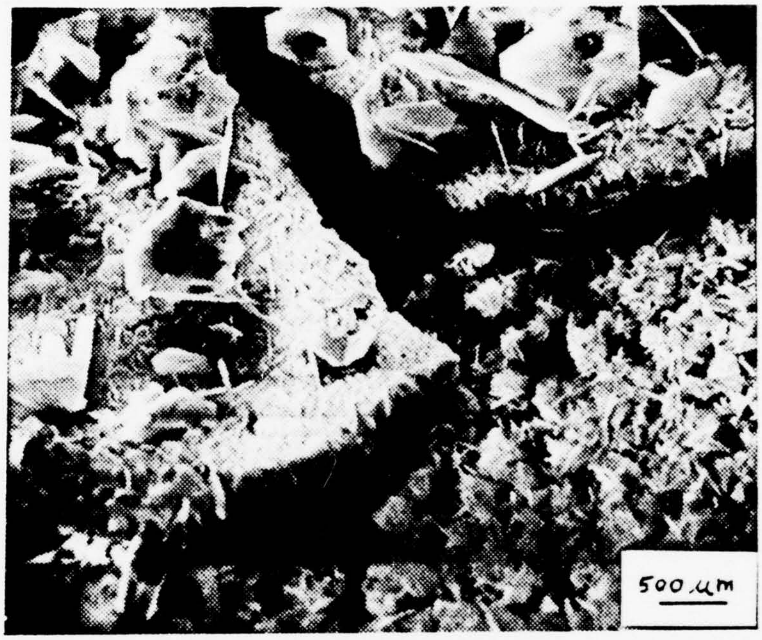

Figure 13

Zinc anode surface after 24 hours static exposure exhibiting a cracking and partially missing outer ZnO layer, 70X (24HZ2)

Figure 14

Zinc anode surface after 24 hours static exposure exhibiting outer and inner ZnO platelet layers, 700X (24HZ2)

Micrographs of a 3 day static exposure sample in which corrosion products rinsed off under a gentle stream of distilled water are shown in Figures 15, 16, 17, 18 and 19. Two distinct layers and morphologies were evident here. Figure 15 exhibits a thick intermediate corrosion product layer still adherent to the zinc anode surface. Figure 16 is a close-up view of the junction of the outer layer and the intermediate layer and also exhibits a portion of the zinc anode surface. It can be seen here that the intermediate layer has a dense mossy corrosion product makeup and appears to be on the order of 50 μm thick. Also in evidence is the appearance that an outer layer of large platelets embedded in a compact layer of smaller platelets are the only platelet layers present. Figure 17 is a view of a 3 day exposure specimen showing platelet layers typical of those that have just been described. Figure 18 shows ZnO platelets embedded in the mossy intermediate product layer. These platelets were most probably left behind as the outer platelet layers rinsed away. Figure 19 is a micrograph of the zinc anode surface exhibiting crystallographic faceting along the hexagonal close packed basal planes. This type of faceting is typical of all zinc anode metal dissolution seen to date. Also evident in this micrograph are ribbon-like corrosion products, first discovered by Luebke [22], who hypothesized that these ribbon-like products usually surround initial dissolution sites on the zinc surface and are eventually grown over as corrosion product growth increases. Figure 18 substantiates the theory that the ribbon-like products remain as corrosion product film growth increases.

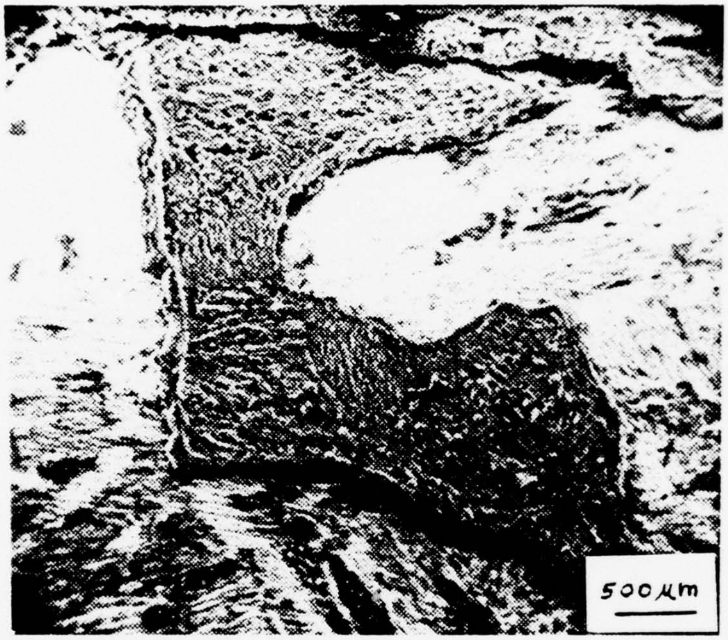

Figure 15

Zinc anode surface after 3 days static exposure showing corrosion product remaining after rinsing, 24X (3DZ1)

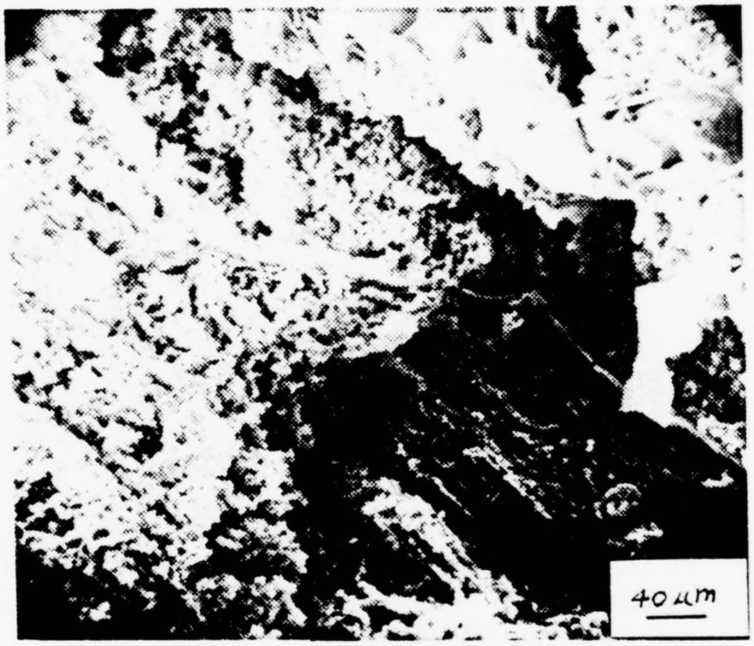

Figure 16

Zinc anode surface after 3 days static exposure showing distinct corrosion product layers, 220X (3DZ1)

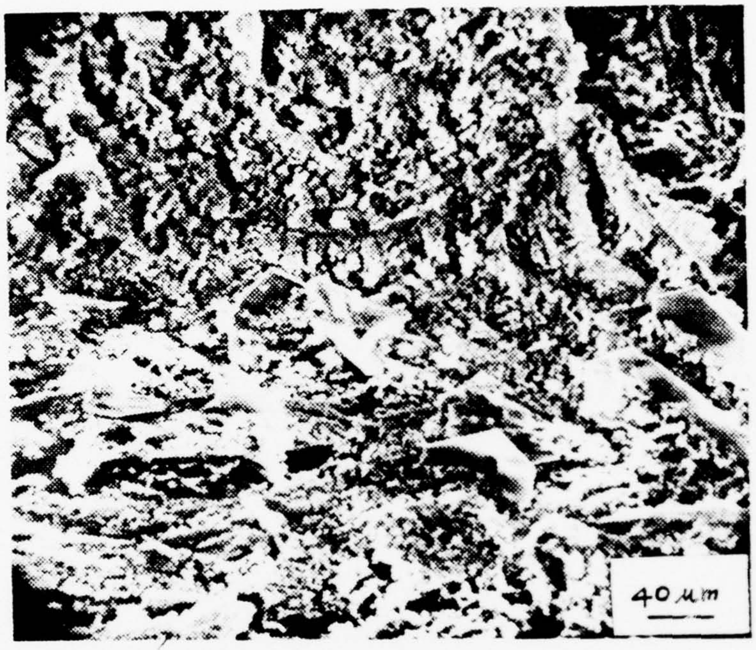

Figure 17

Zinc anode surface after 3 days static exposure, 130X (3DZ2)

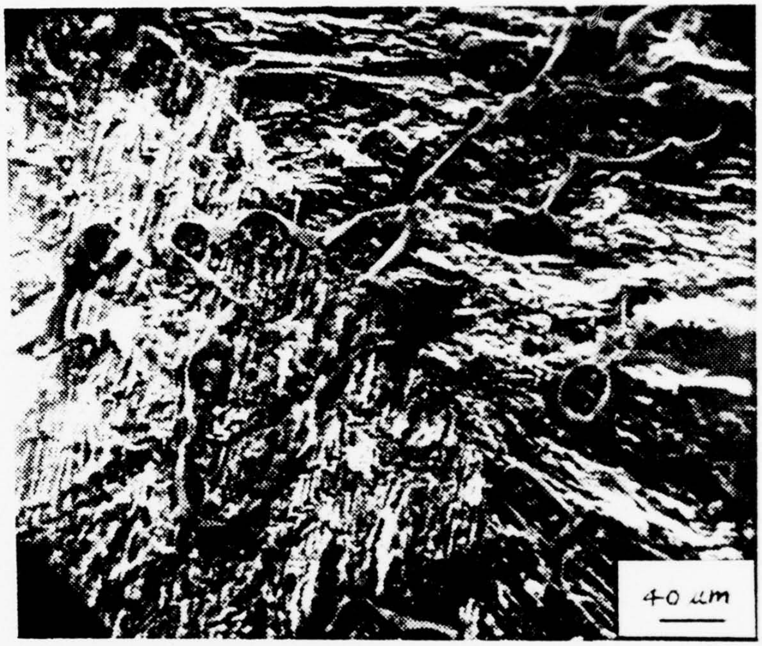

Figure 18

Zinc anode surface after 3 days static exposure showing intermediate corrosion product layer, 233X (3DZ1)

Figure 19

Zinc anode surface after 3 days static exposure showing surface of zinc where intermediate corrosion product layer washed away, 223X (3DZ1)

Figures 20, 21, 22, and 23 are micrographs of 8 day static exposures, which experienced a washing away of corrosion product layers during a gentle rinse. Figure 20 exhibits a platelet layer and an intermediate corrosion product layer which has cracked somewhat. Figure 21 exhibits, from top to bottom, the platelet layer, an intermediate layer and the anode surface. As can be seen here, the intermediate layer is on the order of 150 μm thick as compared to the 50 μm thick intermediate layer on the 3 day static exposure specimen of Figure 16. It should be noted here that the outer platelet layers on the 8 day exposure specimens have not increased noticeably in size over the 3 day exposure specimens; however, the thickness of the intermediate layer has continued to grow. Figure 22 is another view of the intermediate layer and zinc surface. Figure 23 is a closeup of the zinc anode surface, showing the typical crystallographic faceting, ribbon-like corrosion product structures, and remainders of the mossy intermediate layer adhering to the zinc surface. Figure 24 is the PGT 1000 X-ray spectrum taken from the mossy intermediate layer; this reveals the presence of Al, S, and Cl, in addition to the characteristic Zn peaks.

The evident decrease in platelet growth rate as time increases corroborates with Todd's [20] findings. The apparent increase in intermediate layer thickness, however, indicates that sufficient electrolyte is reaching the zinc anode surface and passivation is not taking place. The diffusion of zinc ions through the increasingly thick corrosion product layers

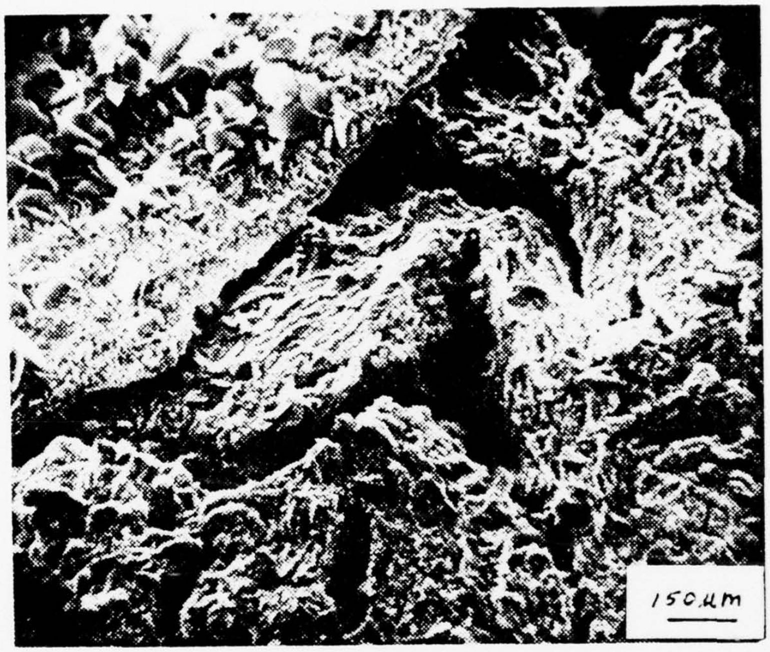

Figure 20

Zinc anode surface after 8 days static exposure, and partial rinsing away of corrosion products, 70X (8DZ1)

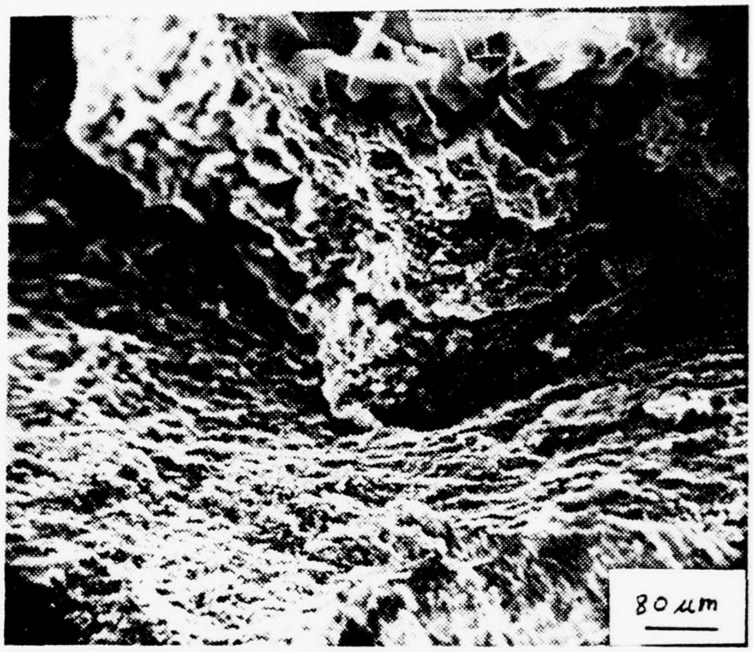

Figure 21

Zinc anode surface after 8 days static exposure, exhibiting thickness of intermediate layer, 130X (8DZ1)

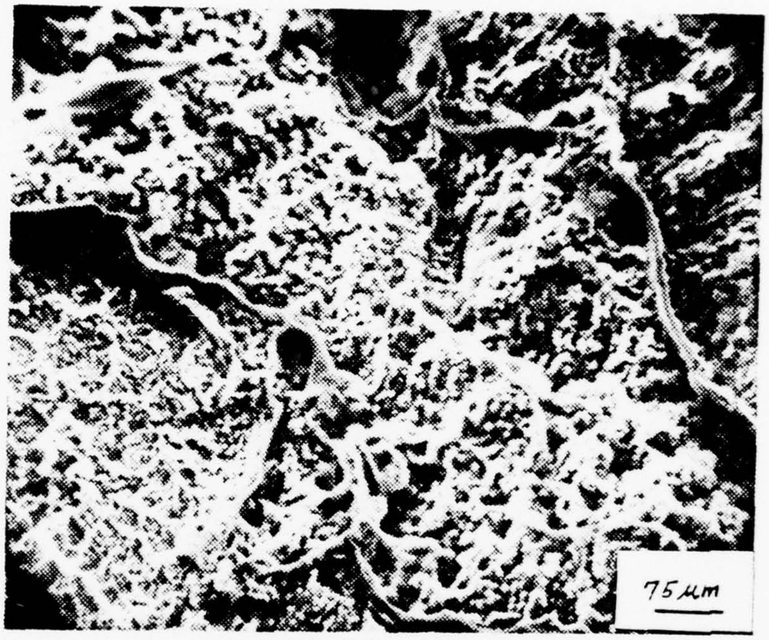

Figure 22

Zinc anode surface after 8 days static exposure, exhibiting the intermediate layer and zinc surface, 140X (8DZ3)

Figure 23

Zinc anode surface after 8 days static exposure and rinsing away of corrosion product, 720X (8DZ3)

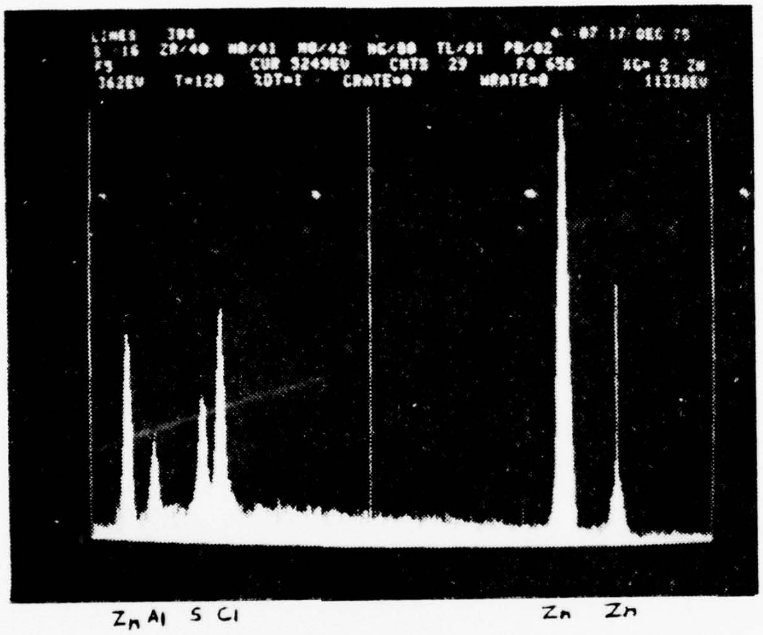

Figure 24

PGT 1000 X-ray spectrum of mossy intermediate layer on 8 day static exposure specimens is the probable cause of platelet growth slowdown. The lack of adherence of the corrosion products at various stages is likely due to stresses set up in platelet layers and the intermediate layer itself as corrosion products continue to form near the zinc surface and the intermediate layer grows outward.

2. Dynamic Exposures

Fluid dynamics seem to play an important role in the behavior of statically-formed anodic corrosion products when subsequently subjected to various velocities and times in the rotating disk electrode apparatus. As stated in the experimental procedures section, the fluid dynamics of the rotating disk electrodes are well-characterized in the literature. The effects of viscosity of the fluid give rise to hydrodynamic boundary layers in which the fluid sticks to the surface of a solid boundary so that no slip or relative motion occurs. Moving away from the solid boundary, the velocity of the fluid increases within the boundary layer until the free stream velocity of the bulk fluid is reached. Laminar boundary layers are characterized by fluid flow which follows lamina or streamlines, whereas turbulent boundary layers exhibit great mixing and extremely large shear stresses on the fluid/solid boundary interface.

The formation of ZnO platelets and other forms of zinc corrosion products is said to depend upon the concentration of ions in the electrolyte above the zinc surface [20]. Farmer and Webb [29] used diffusion theory to explain the dependence of zinc corrosion product formation on electrolyte velocity. They postulated that the corrosion product film growth is dependent upon a critical concentration of zinc ions at the anode surface. The concentration of zinc ions at the surface would depend upon the difference between the rate of removal of ions and the rate of formation of ions by anode dissolution. The rate of ion transport from the surface would depend upon the thickness, δ, of a diffusion layer of electrolyte adjacent to the anode surface. A thicker diffusion layer would inhibit ion removal and accelerate corrosion product formation, as the ion diffusion rate is relatively slow. Under laminar flow conditions, the thickness of the diffusion layer is related to the boundary layer thickness, δ_o, as:

$$\delta = \delta_o / Pr^{1/3} ,$$

where Pr is the diffusion Prandtl number. In the electrolyte environment of this work, $Pr \simeq 10^3$ so that

$$\delta = 0.1\delta_o .$$

As the laminar boundary layer thickness of a plate varies inversely with the square of the bulk fluid velocity, both the diffusion layer and laminar boundary layer thicknesses decrease with fluid velocity increases. This means that ion removal will increase with velocity and corrosion product growth rate will diminish.

In a turbulent boundary layer, extreme fluid mixing and shear stresses will result in a rapid carrying away of ions, and ZnO platelet and underlying corrosion product formation should diminish. The behavior of an electrochemical diffusion layer within a turbulent boundary layer is not well defined [30].

Figure 25 is a micrograph of a 1 hour static exposure specimen showing typical ZnO platelet formation, and Figure 26 is a micrograph of that same specimen after 30 minute dynamic exposure at 100 rpm and the experimentally determined galvanic current density of 5 mA/in^2 (0.775 mA/cm^2). [Unless otherwise noted, all future dynamic exposures shall be at the 5 mA/in^2 (0.775 mA/cm^2) current density.] A marked change was noted in the platelet appearance. There seemed to be a reforming and ion redeposition action taking place. As stated previously, 100 rpm of disk velocity corresponded to the transition from laminar to turbulent flow. Figure 27 exhibits the appearance of a 2 hour static exposure specimen. Figures 28 and 29 are views of a 2 hour static exposure specimen that had been subjected to a dynamic exposure of 100 rpm for 30 minutes. Reforming and redeposition were again evident and appeared to be more marked. Figure 30 is a micrograph of another 2 hour static exposure that had been subjected to a 150 rpm dynamic exposure for 30 minutes. The effects of reforming and redeposition were even more marked at this higher velocity.

The exact nature of this reforming and redeposition action is unknown. It was hypothesized, however, that it is a result of a combination of fluid erosion and continued growth of the ZnO platelets in the turbulent electrolyte. This would indicate that the corrosion product layers formed

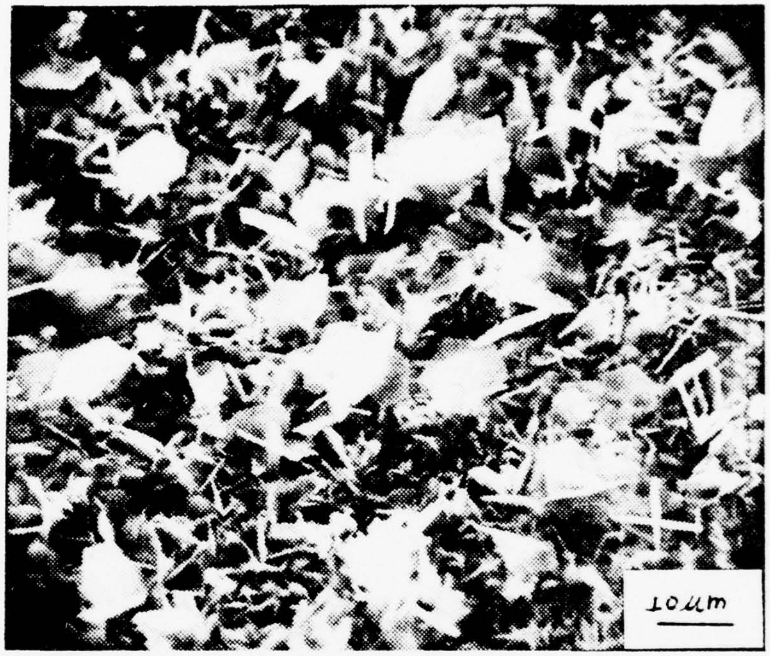

Figure 25

Zinc anode surface after 1 hour static exposure, 1100X (1HZ2)

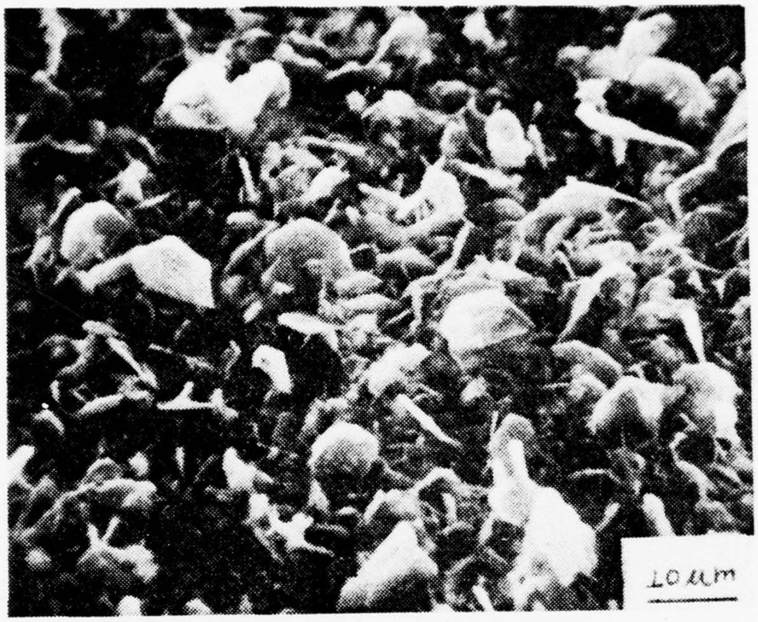

Figure 26

Zinc anode specimen 1HZ2 after 30 min dynamic exposure at 100 rpm and 5 mA/in^2 showing reforming and redeposition, 1240X

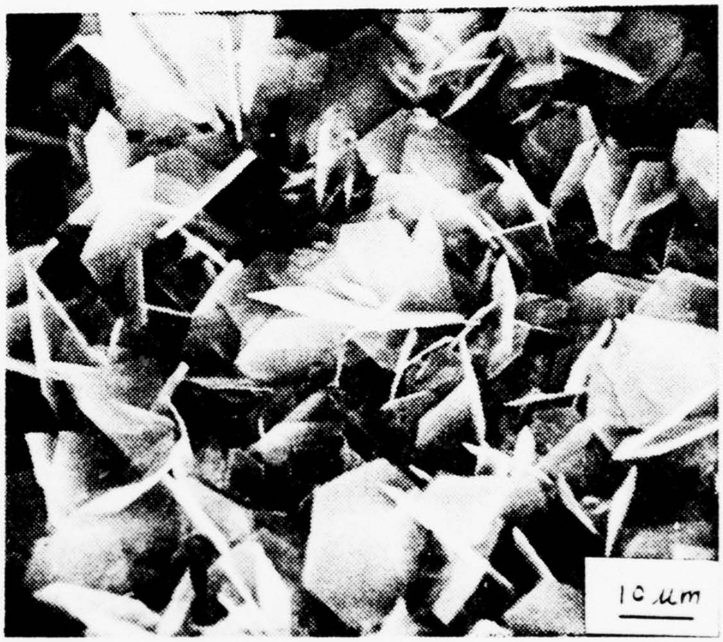

Figure 27

Zinc anode specimen after 2 hour static exposure, 1070X (2HZ1)

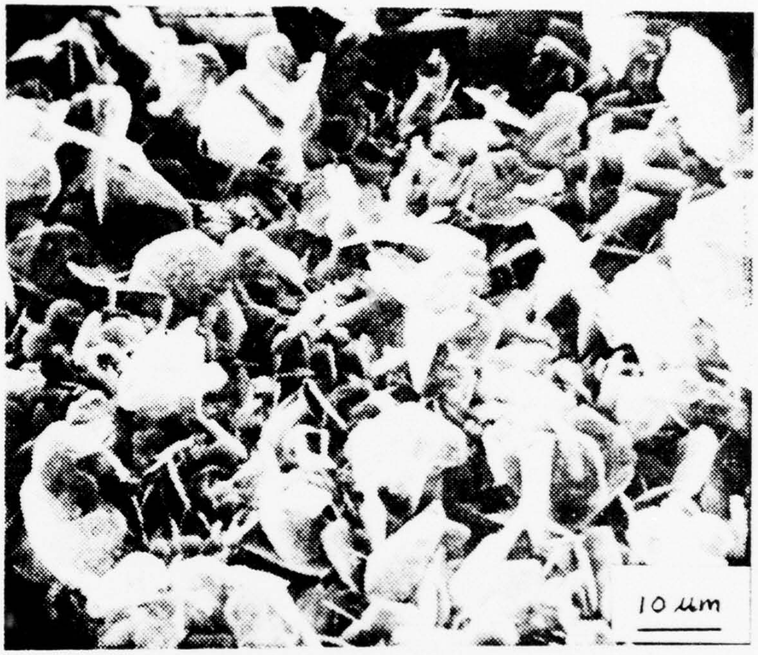

Figure 28

Zinc anode specimen 2HZ1 after 30 min dynamic exposure at 100 rpm and 5 mA/in^2 showing reforming and redeposition, 1200X

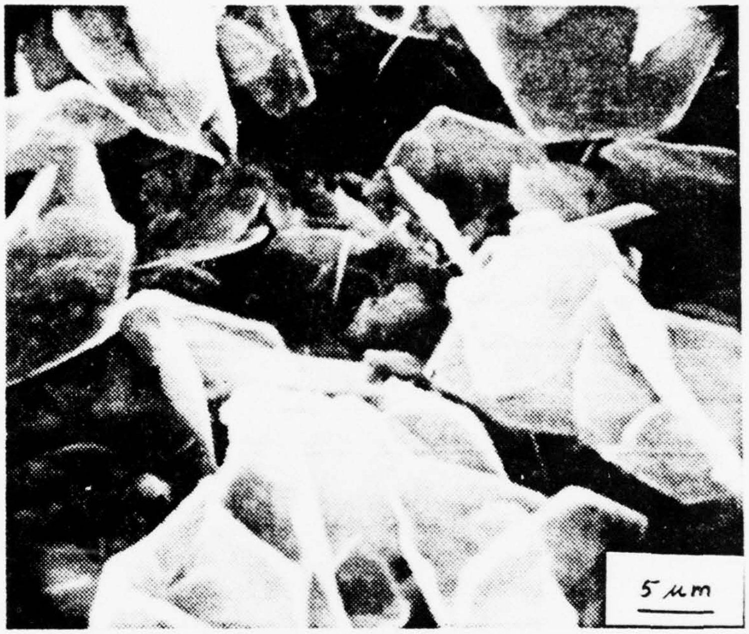

Figure 29

Zinc anode specimen 2HZ1 after 30 min dynamic exposure at 100 rpm and 5 mA/in^2, showing reforming and redeposition, 2200X

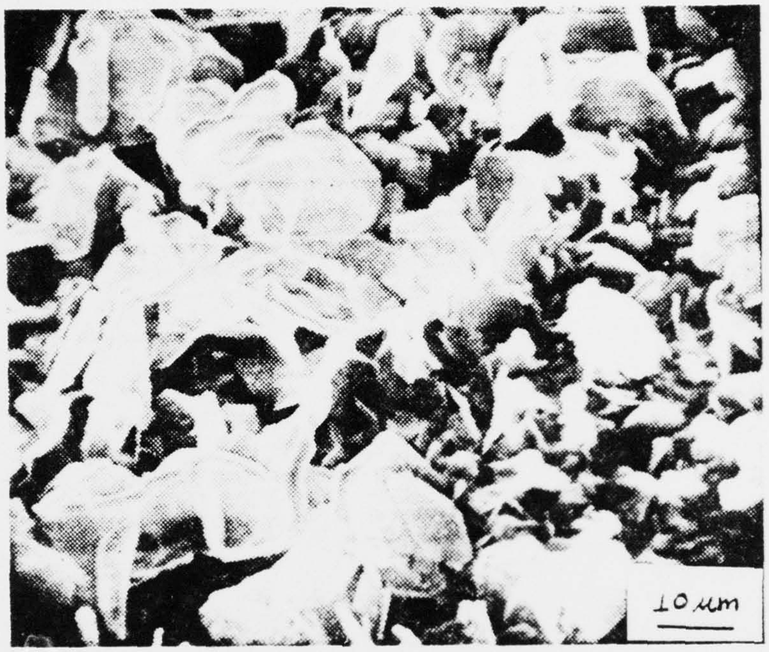

Figure 30

Zinc anode specimen 2HZ2 after 30 min dynamic exposure at 150 rpm and 5 mA/in^2, showing reforming and redeposition, 1130X thus far were not passivating, as Zn^{++} ions were able to diffuse readily through them and into the electrolyte, where redeposition takes place.

An even more dramatic example of this type of action was exhibited in dynamic exposures of samples preexposed 6 hours, as displayed in Figures 31, 32, and 33. Figure 31 shows the structure for a 6 hour static exposure, while Figure 32 is a view of the same specimen after a 1 hour dynamic exposure at 150 rpm. Redeposition and reforming is marked. A closeup of the same specimen is shown in Figure 33. There seems to be a type of shallow pitting, typically found in erosion, and a redeposition of corrosion product in small clumps along the ZnO platelets. Again there is no evidence of passivation, and Zn^{++} ions are apparently readily available for redeposition.

In an attempt to further characterize the phenomena observed here, specimens with 6 hour static exposures were subjected to dynamic exposures with no impressed galvanic current density. Figure 34 exhibits a specimen that was subjected to a dynamic exposure of 30 minutes at 150 rpm with no impressed current. No evidence of redeposition was seen. This corroborates the hypothesis that a certain concentration of zinc ions is necessary for the redeposition process. The absence of evidence of erosion indicates that possibly no mechanical action of erosion was taking place. Therefore, it is hypothesized that the reforming and redeposition process is a function only of electrochemical effects of the flow conditions.

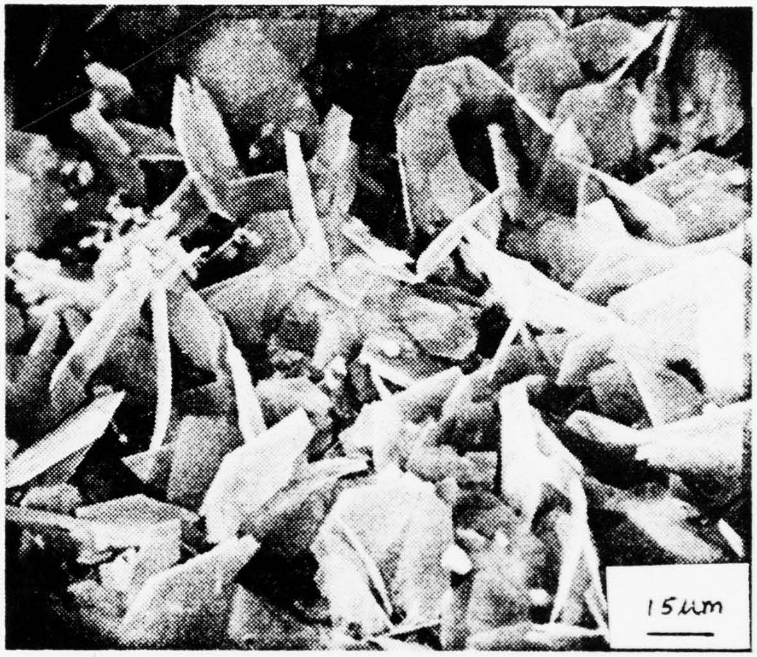

Figure 31

Zinc anode specimen after 6 hour static exposure, 640X (6HZ3)

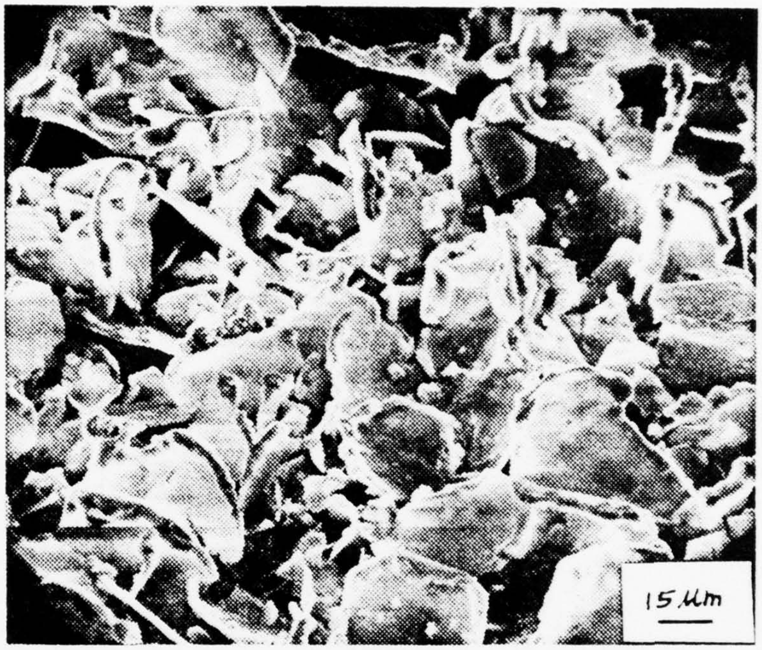

Figure 32

Zinc anode specimen 6HZ3 after 1 hour dynamic exposure at 150 rpm and 5 mA/in^2, showing reforming and redeposition, 540X

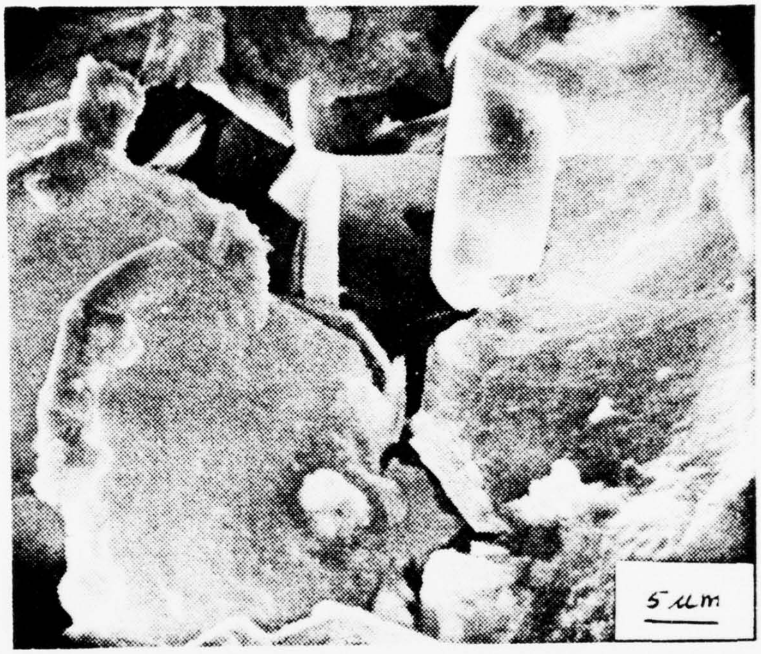

Figure 33

Zinc anode specimen 6HZ3 after 1 hour dynamic exposure at 150 rpm and 5 mA/in^2, showing reforming and redeposition, 2150X

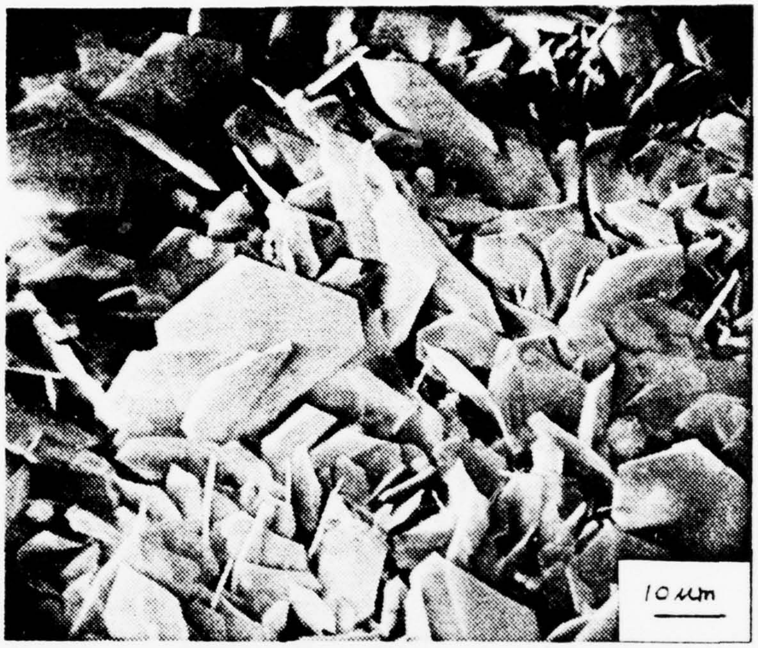

Figure 34

Zinc anode specimen 6HZ2 after 30 min dynamic exposure at 150 rpm and 0 mA/in^2, showing lack of reforming and redeposition, 1050X

It can also be concluded that an increase in exposure time and/or velocity will produce a greater reforming and redeposition action. The results of dynamic exposures of specimens that have undergone static exposures of 12 hours or more differed markedly from the results seen for statically-exposed specimens up to 6 hours. Figure 35 shows a 12 hour static exposure, with somewhat larger platelets than for 6 hour static exposures. As reported by Todd [20], the static ZnO platelet growth rate decreases with time due to decreased ionic diffusion through the thickening corrosion product layers. Figure 36 exhibits the same specimen as in Figure 35 after a dynamic exposure of 1 hour at 150 rpm. No reforming or redeposition is seen, but a new behavior is evident. Figure 37 reveals a portion of the platelet layer and mossy intermediate layer peeled back to reveal a section of the zinc anode surface (which is shown in detail in Figure 38). The start of mossy corrosion product growth is evident on this zinc surface. A micrograph of a 2 hour dynamic exposure at 150 rpm after a 12 hour static exposure is shown in Figure 39. A crust-like formation is evident, along with a portion of the platelet layer removed, as shown in Figure 40 of the same specimen. A closeup of this specimen in Figure 41 reveals a platelet layer over a mossy intermediate layer and the base zinc surface with some mossy growth. From this, it is not obvious whether the crust-like product forms before or after the cracks in the crust develop. Furthermore, the reason for the absence of the ZnO platelets, which once covered the area where the crust now

Figure 35

Zinc anode specimen after 12 hour static exposure, 800X (12HZ3)

Figure 36

Zinc anode specimen 12HZ1 after 1 hour dynamic exposure at 150 rpm, 5 mA/in^2, showing lack of reforming and redeposition, 500X

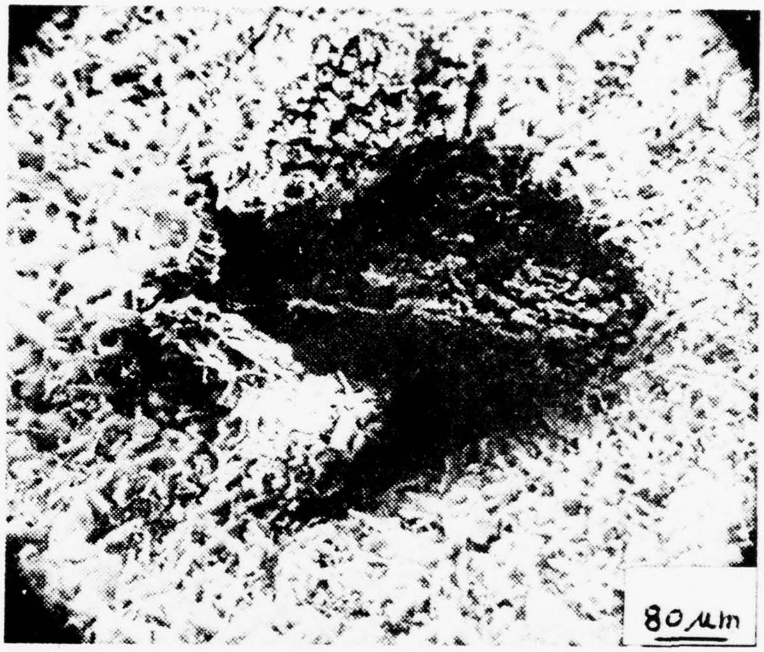

Figure 37

Zinc anode specimen 12HZ1 after 1 hour dynamic exposure at 150 rpm, 5 mA/in^2, showing platelet layer peeled back, 130X

Figure 38

Zinc anode specimen 12H21 after 1 hour dynamic exposure at 150 rpm, 5 mA/in^2, showing zinc surface under peeled back platelet layer, 1300X

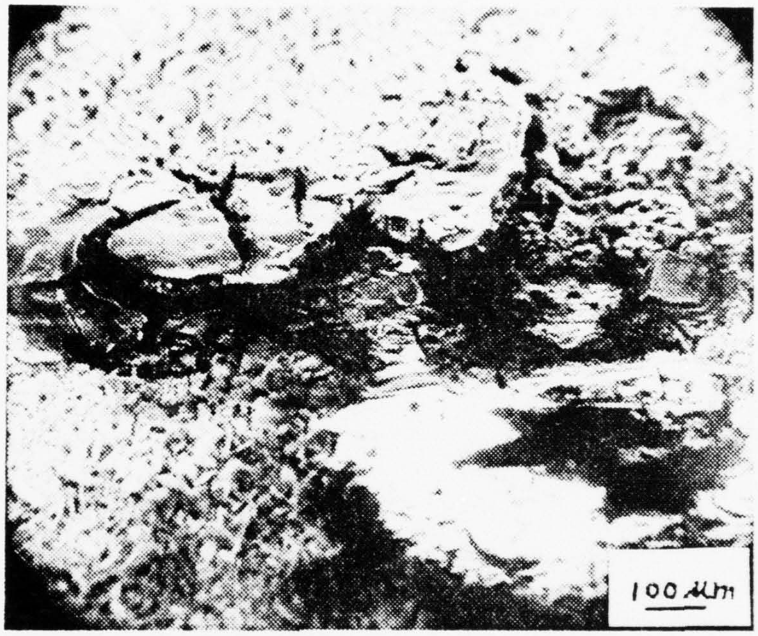

Figure 39

Zinc anode specimen 12HZ2 after 2 hour dynamic exposure at 150 rpm, 5 mA/in^2, showing crust-like product and partial platelet layer removal, 85X

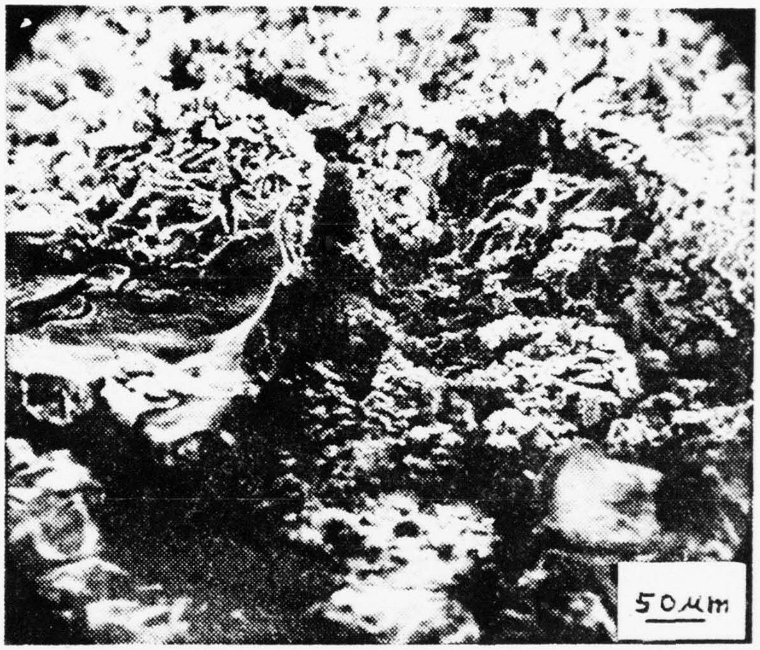

Figure 40

Zinc anode specimen 12HZ2 after 2 hour dynamic exposure at 150 rpm, 5 mA/in^2, showing crust and area of platelet removal, 170X

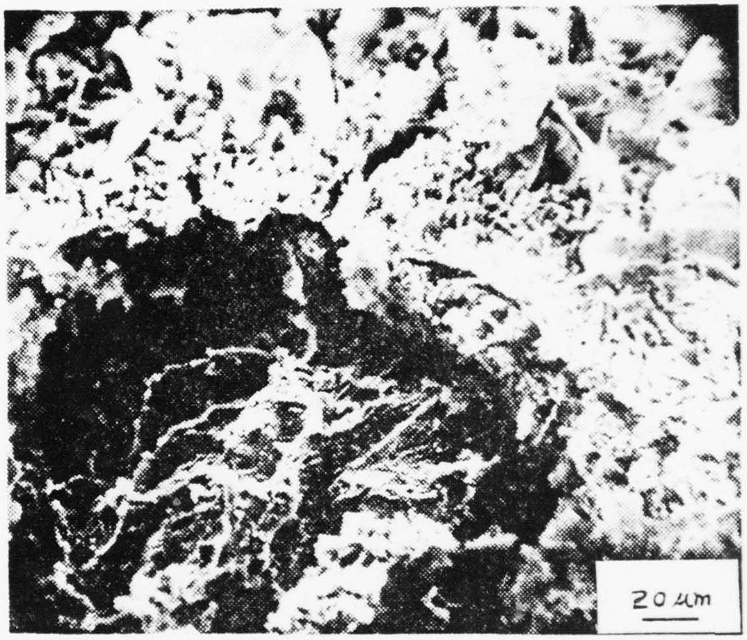

Figure 41

Zinc anode specimen 12HZ2 after 2 hour dynamic exposure at 150 rpm, 5 mA/in^2, showing distinct product layers and underlying zinc surface, 425X

AD-A039 345 NAVAL POSTGRADUATE SCHOOL MONTEREY CALIF F/G 13/10
A SCANNING ELECTRON MICROSCOPE STUDY OF THE CORROSION OF SACRIF--ETC(U)
DEC 76 P W WRIGHT
UNCLASSIFIED NL

2 OF 2
ADA
039345

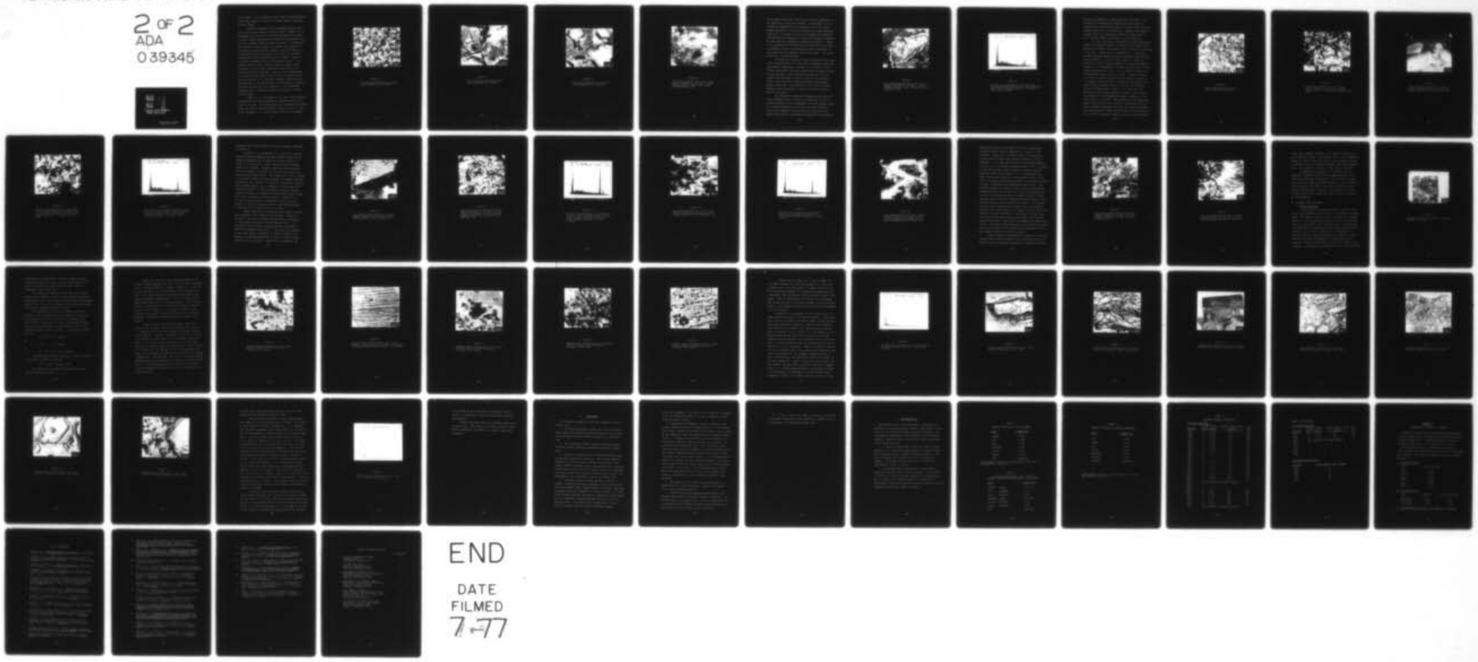

END
DATE
FILMED
7-77

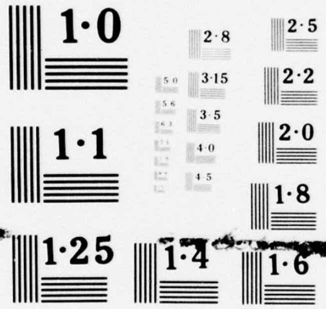

NATIONAL BUREAU OF STANDARDS
MICROCOPY RESOLUTION TEST CHART

is not known. It is evident, however, that increased exposure time (from 1 hour to 2 hours at 150 rpm) results in greater platelet damage.

Further investigation using specimens exposed statically for 36 hours reveals a similar result. Figure 42 is a micrograph of a 36 hour static exposure specimen that shows a layer of large individual and clustered ZnO platelets forming over a compact layer of smaller platelets. A closeup of this platelet network (Figure 43) reveals the denseness of the underlying fine platelet network. Also in evidence is a formation of darker platelets which seem to be oriented more parallel with the underlying zinc surface. Figure 44 is another micrograph of this same platelet growth. It is believed that the more conductive nature of these darker platelets is due to their orientation with regard to the electron beam within the SEM. Platelets more perpendicular to the SEM electron beam are better able to conduct or pass the electrons due to the platelet thinness, while platelets more parallel to the beam present a thicker path for electron transport and are thus less conductive. Less conductive platelets eject secondary electrons more readily to form a brighter image.

Figure 45 is a micrograph of a 36 hour static exposure specimen that has been subjected to a dynamic exposure of 2 hours at 150 rpm. The cracking and crust formation are greater than that noted in the same dynamic exposures of the 12 hour static specimens. It is also evident that not all cracking

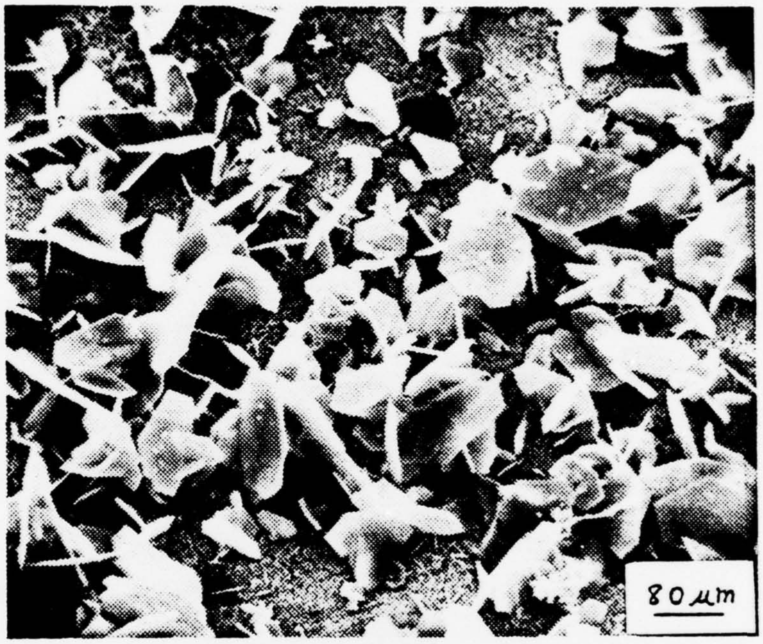

Figure 42

Zinc anode specimen after 36 hour static exposure, 125X (36HZ3)

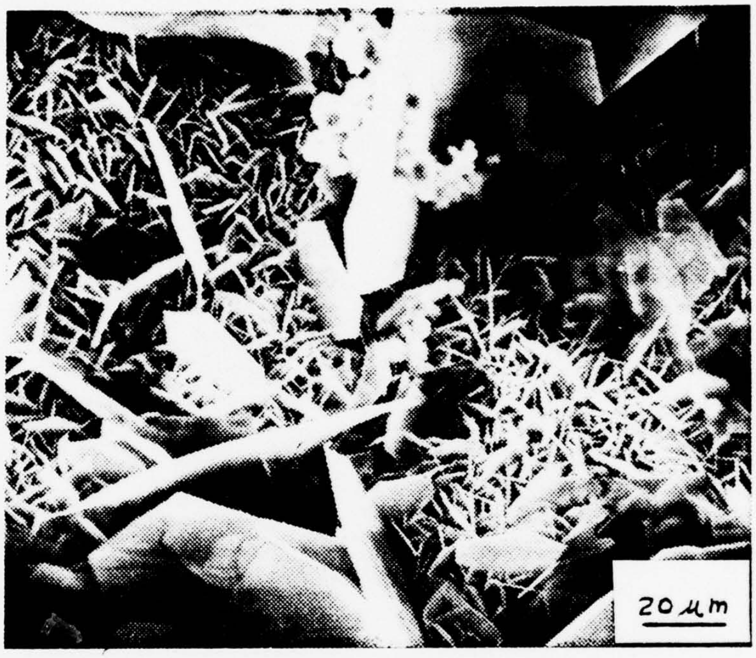

Figure 43

Zinc anode specimen after 36 hour static exposure, 610X (36HZ3)

Figure 44

Zinc anode specimen after 36 hour static exposure, 610X (36HZ2)

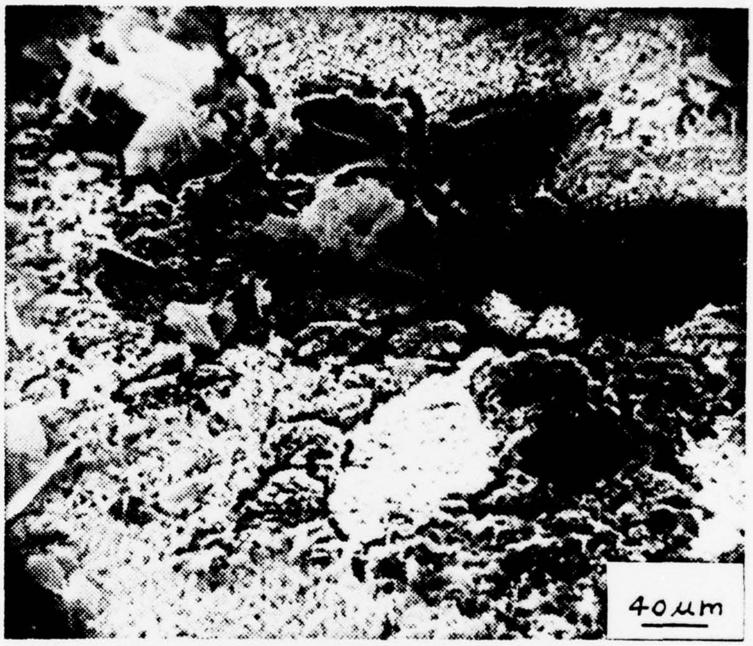

Figure 45

Zinc anode specimen 36HZ2 after 2 hour dynamic exposure at 150 rpm, 5 mA/in^2, showing platelet layer cracking and crust formation, 240X of the dense smaller platelet layer has been accompanied by the formation of crust-like products. Additionally, no reforming or redeposition was evident here or in any longer dynamic exposures of statically exposed zinc anode specimens. Figure 46 is a closeup of an area of cracked dense platelet area showing the formation of a crust-like product surrounded by what seem to be gradually disappearing platelets. Figure 47, a photograph of the PGT-1000 X-ray spectrum of the crust-like product, shows a strong magnesium peak in addition to zinc peaks that are somewhat smaller than usual. This revelation will be explained later.

The increase in platelet layer cracking of the 36 hour static specimens over the 12 hour static specimens, under the same dynamic conditions, is thought to be related to the increased intermediate corrosion product layer thickness of the 36 hour specimens. This increased intermediate layer has probably created greater tensile stresses in the platelet layers, which resulted in more pronounced cracking under dynamic conditions. The formation of crust-like corrosion products could be related to cracks in the dense platelet layer at this point.

The absence of reforming and redeposition action for static exposures above 12 hours is probably due to the increased thickness of the intermediate corrosion product layer, which causes diffusion of zinc ions to be more difficult. Ions which do manage to diffuse into the electrolyte are rapidly swept away by the existing turbulent flow conditions

Figure 46

Zinc anode specimen 36HZ2 after 2 hour dynamic exposure at 150 rpm, 5 mA/in^2, showing platelet layer cracking and crust formation, 500X

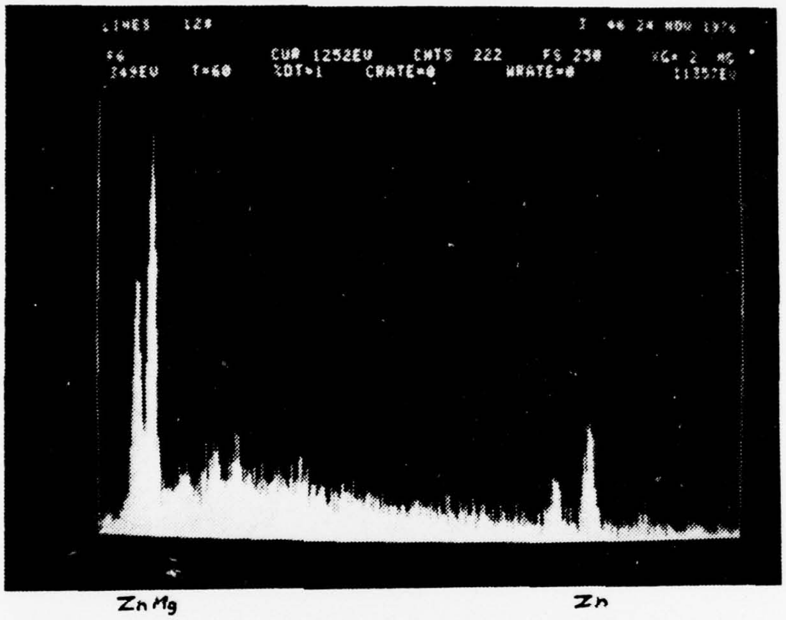

Figure 47

PGT-1000 X-ray spectrum of the crust-like corrosion product found on zinc anode specimen 36HZ2 after a dynamic exposure of 2 hours at 150 rpm, 5 mA/in^2

before any reforming or redeposition can take place. The absence of a reforming and redeposition action might be interpreted as promoting the onset of a passivating corrosion product layer on the zinc specimens. However, since there is evidence that the intermediate corrosion product layer is still growing, anodic dissolution is still occurring.

Up until this point, the behavior of static corrosion products in dynamic exposure situations had not been investigated in the laminar flow regime of the rotating disk electrode (< 100 rpm). Figure 48 is a micrograph of a 2 day static exposure specimen showing the same corrosion product morphology of Figure 42, a 36 hour static exposure. Again, the evidence is that ZnO platelet growth has slowed considerably. Figure 49 is a micrograph of the same specimen after a 3 hour dynamic exposure at 100 rpm. This is further evidence that reforming and redeposition have ceased. Figure 50 reveals that platelet layer cracking and spalling have occurred on this sample, and Figure 51 is a closeup of the nodular clustered corrosion product found in the areas where platelet layers have spalled off. Figure 52 is a PGT-1000 X-ray spectrum of the corrosion product of Figure 51 and reveals the presence of a strong magnesium peak in addition to the characteristic zinc peaks. Mor and Beccaria [16] found that $MgSO_4$, $ZnSO_4$ and $CaCO_3$ were likely to precipitate from synthetic seawater electrolyte and onto zinc corrosion products. Such precipitation of $MgSO_4$ could account for the presence of Mg in the X-ray spectrum. $MgSO_4$ may exist as a precipitate

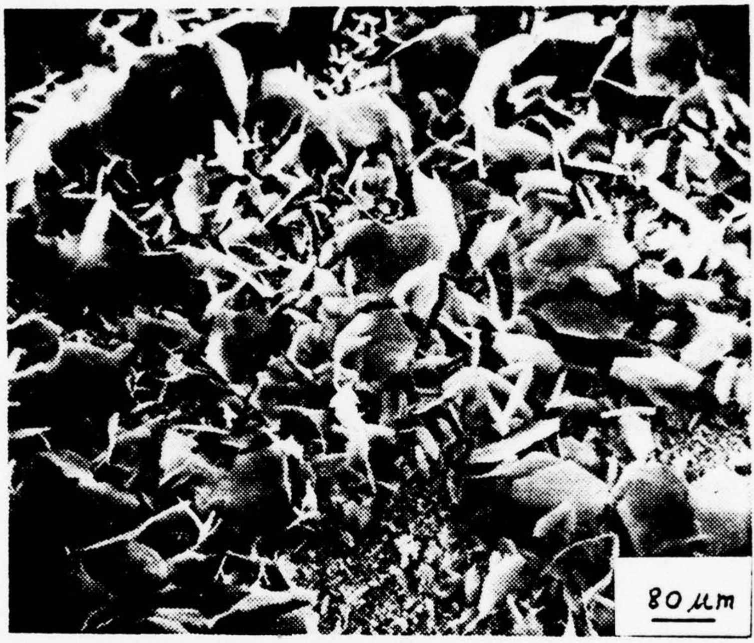

Figure 48

Zinc anode specimen after 2 day static exposure, 120X (2DZ1)

Figure 49

Zinc anode specimen 2DZ1 after 3 hour dynamic exposure at 100 rpm, 5 mA/in^2, showing lack of reforming and redeposition, 220X

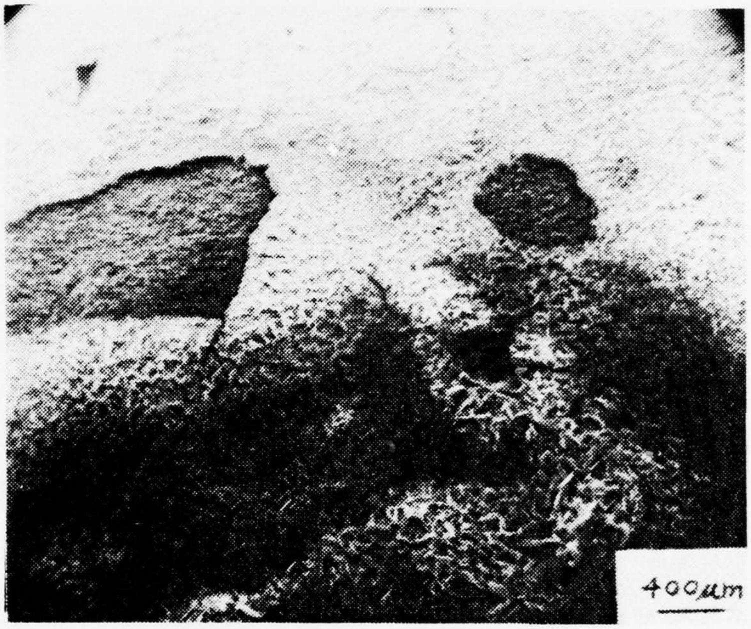

Figure 50

Zinc anode specimen 2DZ1 after 3 hour dynamic exposure at 100 rpm, 5 mA/in^2, showing areas of platelet removal, 24X

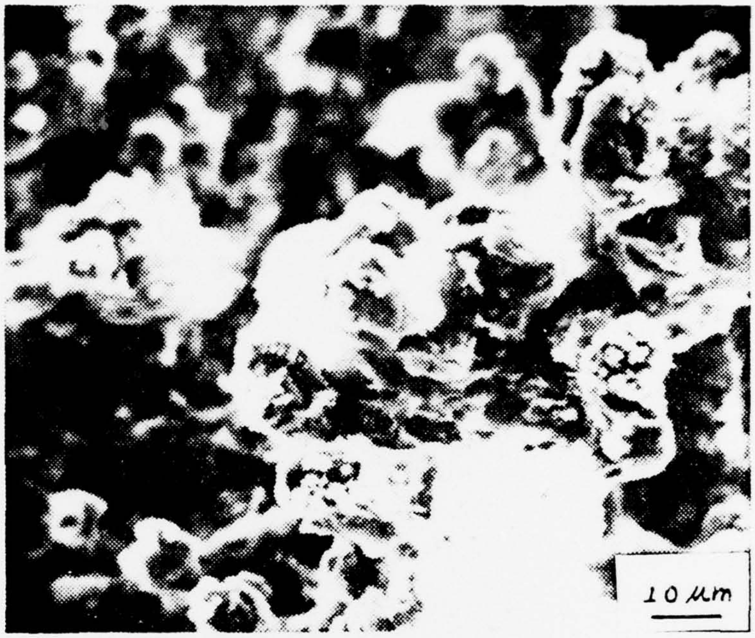

Figure 51

Nodular corrosion product cluster found in area where platelet layer spalled off of zinc anode specimen 2DZ1 after 3 hour dynamic exposure at 100 rpm, 5 mA/in^2, 1040X

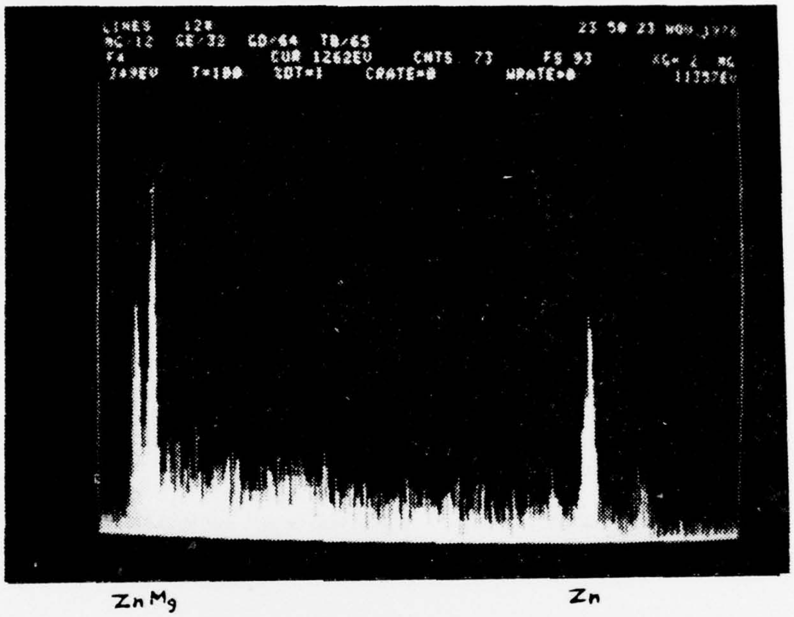

Figure 52

PGT-1000 X-ray spectrum of nodular cluster corrosion product found in spalled area of zinc anode specimen 2DZ1 after 3 hour dynamic exposure at 150 rpm, 5 mA/in^2

entrapped within the growing zinc corrosion product evidenced in Figure 51.

Figure 53 is a micrograph of a 2 day static exposure specimen that has undergone the same dynamic exposure as the Figure 50 specimen, but at triple the current density (15 mA/in^2 or 2.325 mA/cm^2). Again, spalled corrosion product areas are in evidence. However, almost the entire platelet layer had spalled off (Figure 54) revealing the nodular corrosion product found earlier. The growth rate of the 15 mA/in^2 (2.325 mA/cm^2) nodular corrosion product was greater than that observed for the 5 mA/in^2 (0.775 mA/cm^2), as would be expected. This increased growth rate is thought to be the cause of the increased spalling. As the intermediate corrosion product layer grew faster, the adherence of the platelet layers became even less, and greater spalling occurred. Figure 55 is a PGT-1000 X-ray spectrum for the nodular cluster corrosion product of Figure 54 and again shows a large magnesium peak in addition to the characteristic zinc peaks.

Dynamic exposures in the laminar flow regime exhibited more pronounced crust formation and cracking. Figure 56 reveals a 2 day static exposure specimen that had undergone a 3 hour dynamic exposure at 50 rpm (laminar flow). The evidence of platelet layer cracking and crust formation is even more pronounced than before. A PGT-1000 X-ray spectrum of the crust formed in Figure 56 is shown in Figure 57 and reveals a strong magnesium peak, as well as stronger sulfur, chlorine and calcium peaks. Figure 58 is a closeup of the

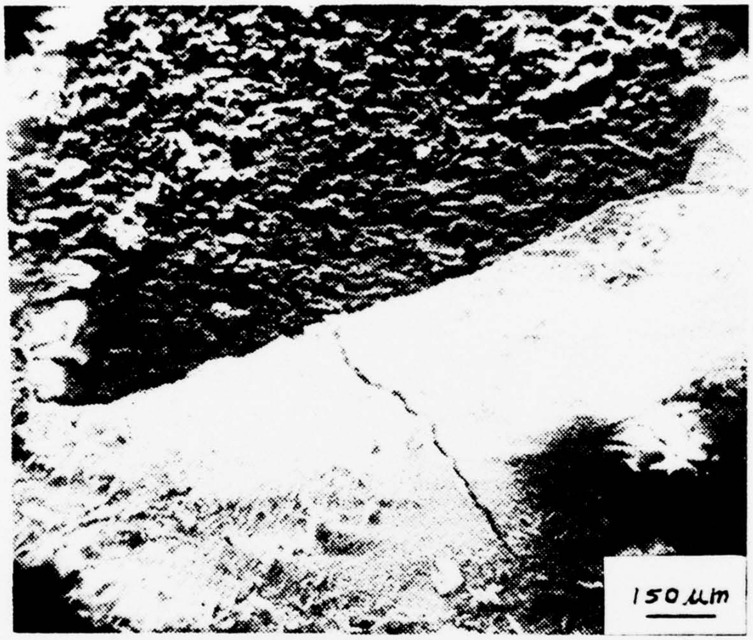

Figure 53

Zinc anode specimen 2DZ3 after 3 hour dynamic exposure at 100 rpm, 15 mA/in^2, showing platelet area spalling, 66X

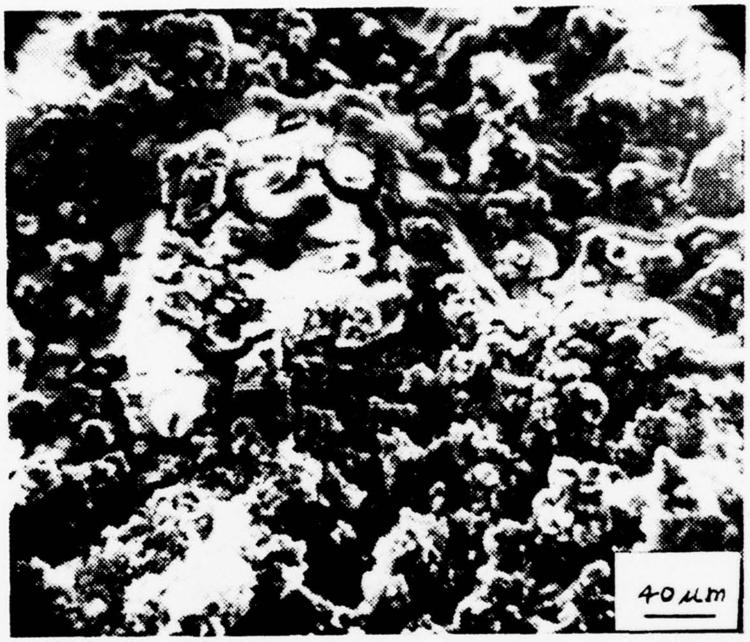

Figure 54

Zinc anode specimen 2DZ3 after 3 hour dynamic exposure at 100 rpm, 15 mA/in^2, showing the nodular cluster corrosion product within areas of platelet area spalling, 260X

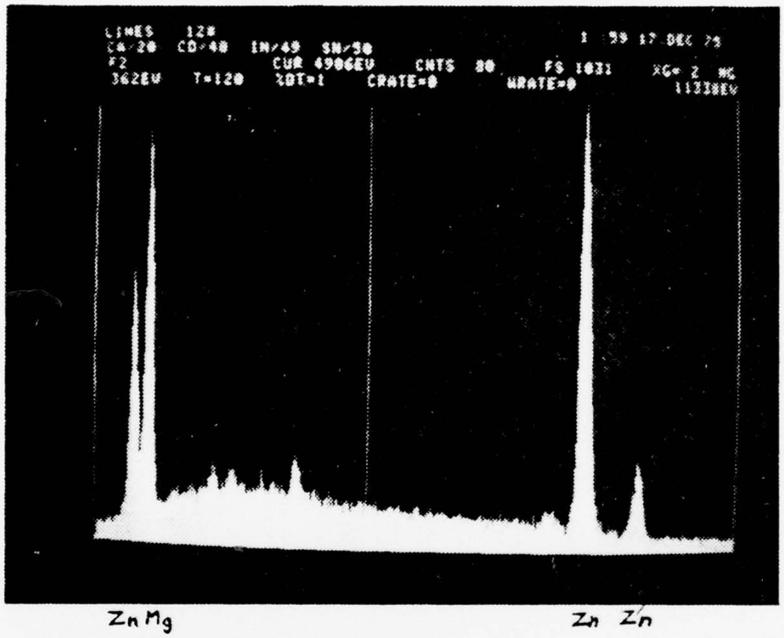

Figure 55

PGT-1000 X-ray spectrum of the nodular cluster corrosion product within spalled areas of anode specimen 2DZ3 after a 3 hour dynamic exposure at 100 rpm, 15 mA/in^2

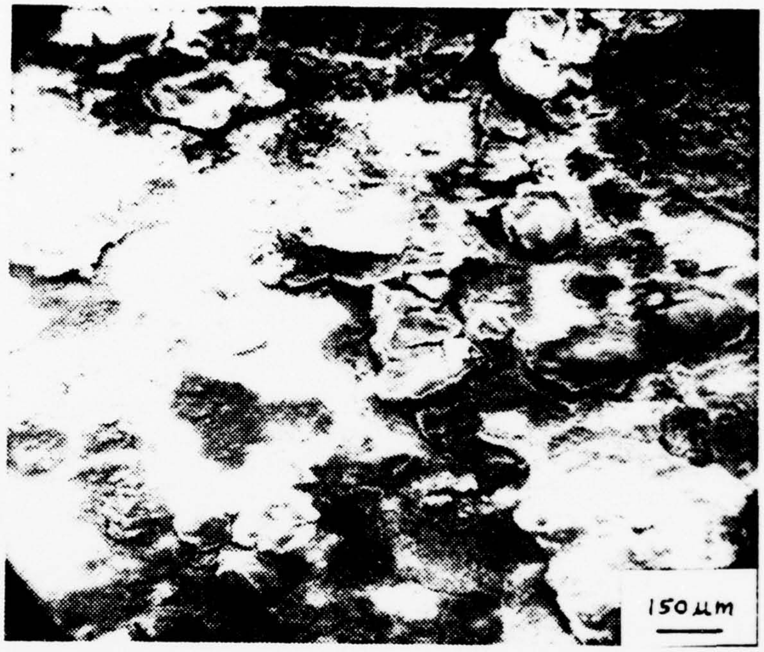

Figure 56

Zinc anode specimen 2DZ2 after 3 hour dynamic exposure at 50 rpm, 5 mA/in^2, showing extensive crust formation, 66X

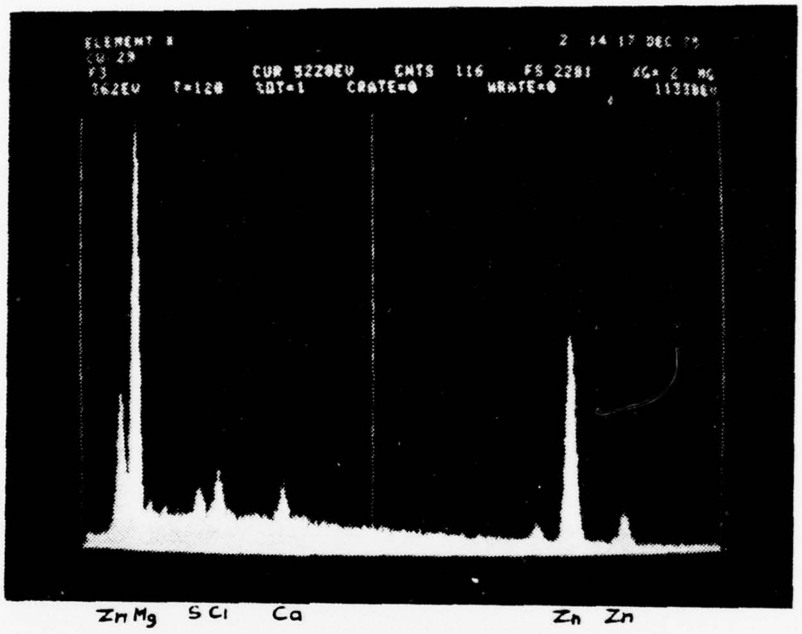

Figure 57

PGT-1000 X-ray spectrum of crust-like products on zinc anode specimen 2DZ2 after 3 hour dynamic exposure at 50 rpm, 5 mA/in^2

Figure 58

Zinc anode specimen 2DZ2 after 3 hour dynamic exposure at 50 rpm, 5 mA/in^2, showing cracked crust formation and mossy intermediate layer below, 200X specimen of Figure 56 and reveals the mossy intermediate corrosion product layer in addition to an absence of ZnO platelets. Figure 59 is a further view of the specimen at a point where the crust-like products interface with ZnO platelets. It is here that the key to ZnO platelet disposition and crust-like product formation seems to lay. In Figure 59, the ZnO platelets seem to reform or dissolve into the developing crust-like formation. It is hypothesized that under laminar flow conditions, the presence of ions at the corrosion product/electrolyte interface is sufficient to allow the type of reforming and redeposition seen earlier. This reforming engulfs the nearby platelets and any precipitated compounds present and results in a crust-like formation that is lower in surface area than the original products. Crust cracking results from this shrinking corrosion product layer, and more paths for ionic diffusion are opened. The original platelet layer cracking seen initially here in dynamically exposed 12 hour static exposure specimens, is most likely the catalyst for crust formation. As the platelet layers crack, zinc ions are allowed to diffuse more readily into the near surface electrolyte, initiating the reforming and redeposition action. It should be noted here that crust formation has been shown to be evident under turbulent flow conditions, but to a much smaller extent, as would be expected.

Another example of turbulent flow effects on corrosion products may be seen in Figure 60 which shows the results of platelet layer cracking and spalling of a dynamically exposed

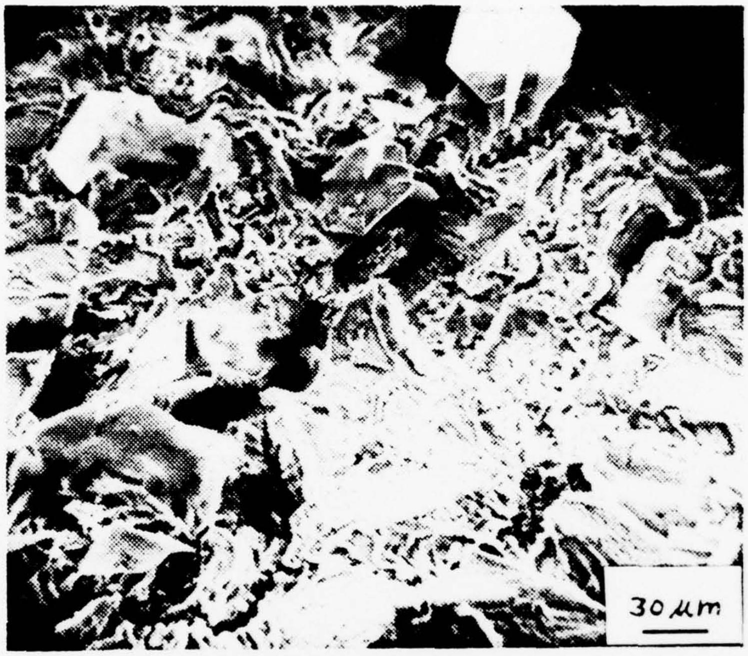

Figure 59

Zinc anode specimen 2DZ2 after 3 hour dynamic exposure at 50 rpm, 5 mA/in^2, showing platelets reforming into crust formation, 325X

Figure 60

Zinc anode specimen 3DZ2 after 3 hour dynamic exposure at 150 rpm, 5 mA/in^2, showing spalled off platelet area, 130X

3 day static exposure specimen. This dynamic exposure was at 150 rpm for 3 hours. The tendency here was for intermediate corrosion product growth and platelet layer cracking followed by portions of the less adherent platelet layer being carried away. This behavior is typical of that seen in this work.

In summary, there appears to be distinct but not necessarily separate zinc corrosion product behavior in the laminar and turbulent flow regimes. This behavior is dependent upon prior corrosion product morphology, time of previous static exposure, and velocity and time of dynamic exposure. Whatever the behavior, in any case the tendency is for the MIL-SPEC-A-18001H zinc sacrificial anode to avoid passivation by some mechanism.

B. ALUMINUM ANODE SPECIMENS

1. Static Exposures

Investigation of aluminum sacrificial anodes in this thesis was undertaken as a corollary to the primary zinc anode work. The aluminum sacrificial anode specimens were prepared exactly as the zinc anode specimens except that the specimen sides were not painted with insulating dope. Aluminum anode specimens were only subjected to static exposures for periods of time of up to 2 days. Figure 61 is a micrograph of a specimen that was statically exposed for a period of 2 days. Striations of corrosion products and much pitting are in evidence. Pitting is particularly severe at the edges of the specimen. The striations are parallel to what was the vertical

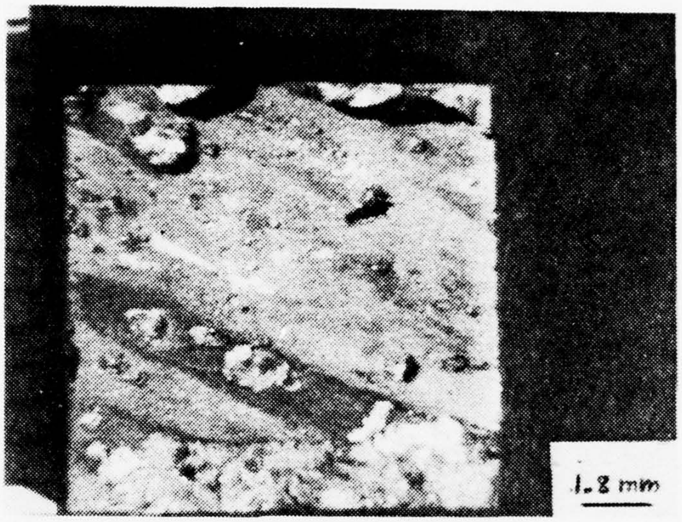

Figure 61

Aluminum anode specimen after 2 day static exposure, 6X (2DA1) orientation of the specimen in the static exposure beaker. Exposures for periods of time of up to 2 days showed no increase in pitting sites with time but showed a distinct enlargement of pits with time.

The absence of attack for large areas of the anode surface was a reason for concern of Naval Research Laboratory investigators [14]. It was felt that large areas of the anode might be "lost" due to the irregular pitting pattern, without serving their cathodic protection function.

The initiation of pitting in normally passivated aluminum is most probably due to the breakdown of the Al_2O_3 passivating film by the Cl^- ion present in seawater [31]. Once the film is penetrated, a series of autocatalytic reactions result in pit growth. A recent work by Galvele [26] presented a model of such pit growth. The reactions evident here are

$$Al \rightarrow Al^{+++} + 3e^- \text{ (anode)}$$

and

$$2H^+ + 2e^- \rightarrow H_2 \text{ (cathode)}$$

or

$$O_2 + 4H^+ + 4e^- \rightarrow 2H_2O \text{ (cathode).}$$

The aluminum dissolution reaction is further followed by a hydroysis reaction of the type

$$Al^{+++} + 3H_2O \rightarrow Al(OH)_3 + 3H^+$$

The resulting continuing acidification of the pit maintains the pitting action.

Figure 62 is a view of the corrosion product on the surface of anode specimen 1DA1 after a 24 hour static exposure. A mossy corrosion product is evident. Figure 63 is a view of the same specimen in a striated area with few corrosion products. Only small nodules of corrosion product appear here, along with specimen sanding marks. It is not evident, from sample observation, why the striations appear. They could be related to dissolution sites and corrosion product formation at those sites. However, it is evident in Figure 61 that large pits have formed in areas relatively free of corrosion products. Additional investigation should be done on this behavior.

Figure 64 shows the corrosion product formed in a denser striation after 2 days static exposure, and Figure 65 is a magnified view of the same product, evidencing clusters of tiny nodules. Figure 66 is another view of this striation area, showing a cracked film of the tiny nodules seen previously. It is believed that this prduct film cracked upon drying, as no dynamic exposure conditions were imposed. Figure 67 is a PGT-1000 X-ray spectrum of the corrosion product of Figure 65, evidencing a sulfur peak in addition to the stronger aluminum peak. This indicates only that the corrosion product compound contains these elements but does not give the stoichiometry. The tenaciousness and exact composition of these corrosion products are unknown and are possible subjects for future research.

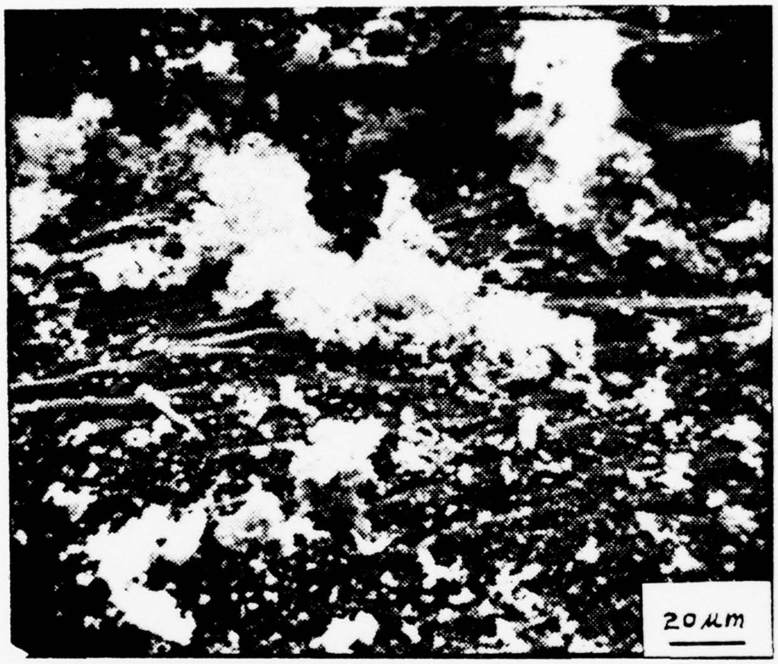

Figure 62

Aluminum anode specimen after 1 day static exposure showing corrosion product in striation, 550X (1DA1)

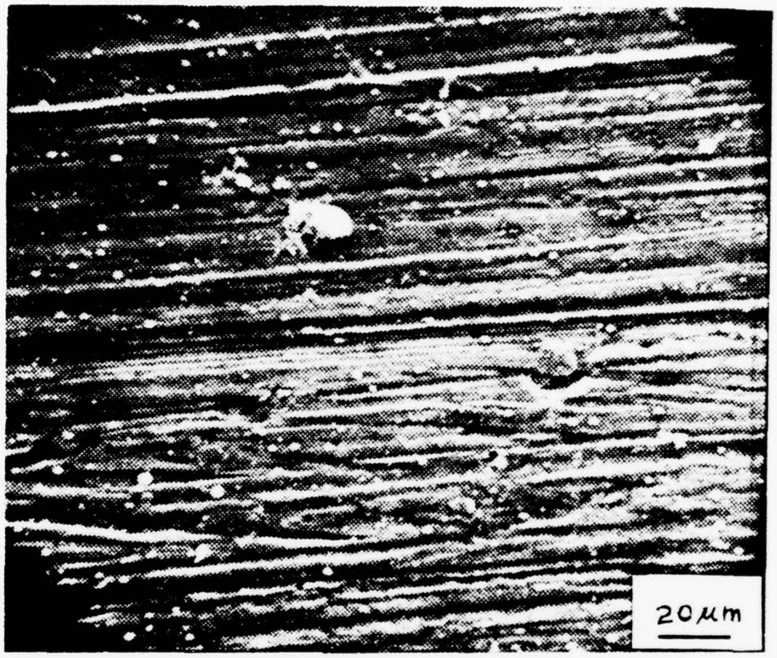

Figure 63

Aluminum anode specimen after 1 day static exposure showing corrosion product in striation of least corrosion product density, 530X (1DA1)

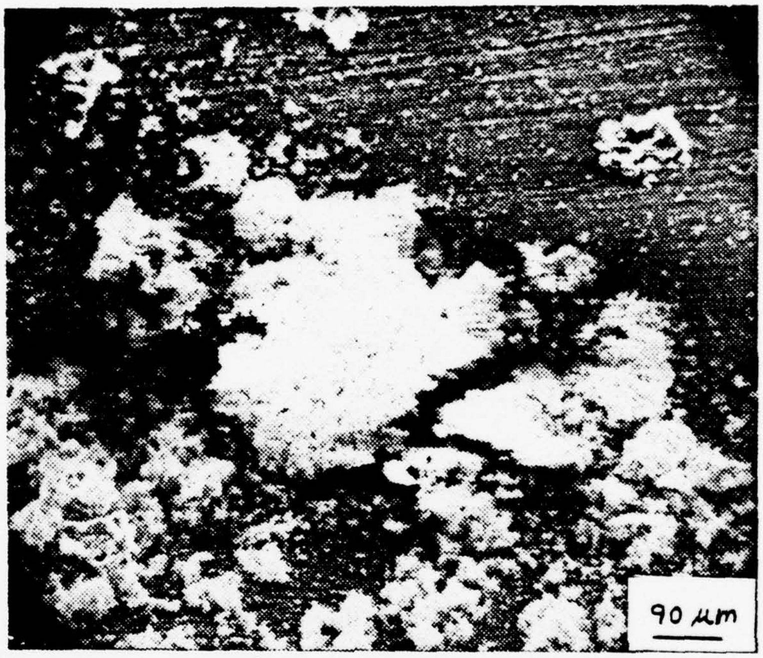

Figure 64

Aluminum anode specimen after 2 day static exposure showing corrosion product in striation, 110X (2DA1)

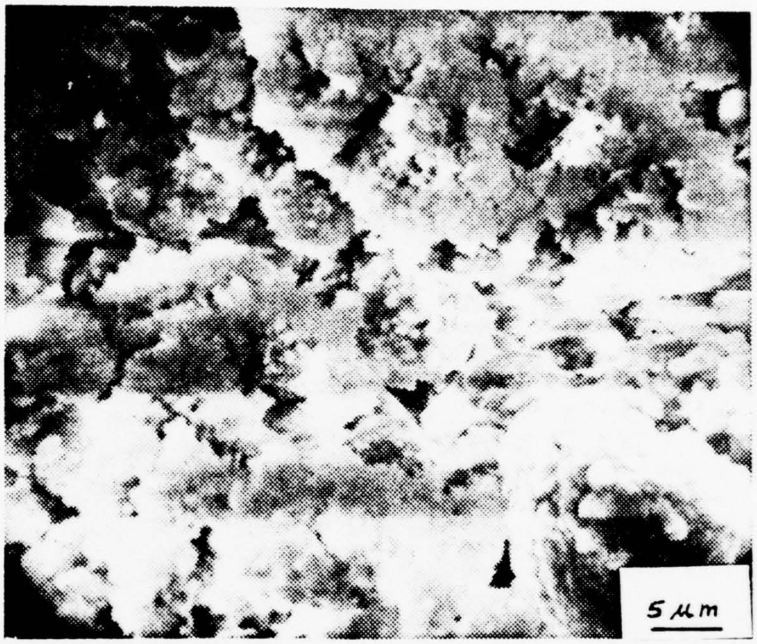

Figure 65

Aluminum anode specimen after 2 day static exposure showing corrosion product in striation, 2100X (2DA1)

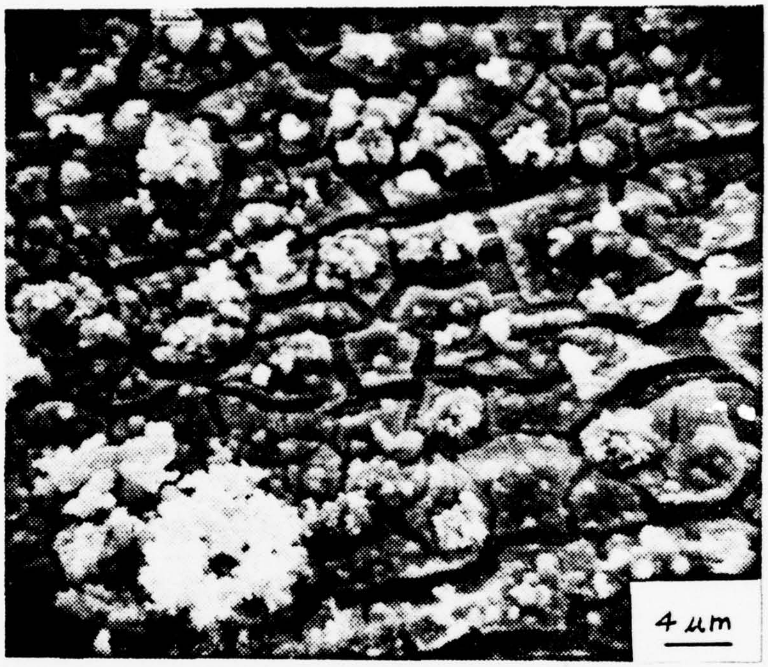

Figure 66

Aluminum anode specimen after 2 day static exposure showing corrosion product in striation, 2500X (2DA1)

A closer view of a small pit is seen in Figure 68. This anode specimen was statically exposed for 2 days, and a nodular mossy corrosion product is evident within the pit. The pitting action appears to be progressing outward as well as downward, undercutting the still passivated surface of the anode. Areas of surface metal can be seen to be loosening and falling into the pit or being consumed in the dissolution process. This sequence would explain the observed enlargement of pits with time.

Figure 69 is a micrograph of the bottom of a pit in anode specimen 1DA1 after 1 day static exposure. Grain boundaries seem to be evident (the raised lighter-colored features that appear almost as hedgerows). There are also numerous cones and hills in evidence, with some corrosion product or deposit clinging to them. Figure 70 is a micrograph of a pit area in anode specimen 1DA1 after cleaning the corrosion products from the specimen in an ultrasonic bath of distilled water. The pitting pattern shows dissolution on the sides of the pits as well as the bottom. Figure 71 displays a portion of a pit in specimen 2DA1. The probable grain boundaries are seen to be decorated by the previously mentioned cones or hills. Additionally, the black matrix seems to be anodic to the grain boundaries. Figure 72 shows the side of such a pit and evidences the same attack pattern as seen at pit bottoms. Figure 73 is a higher magnification of the specimen of Figure 72 and evidences the black matrix and more cathodic grain boundaries. Figure 74 is another view of the cones or hills

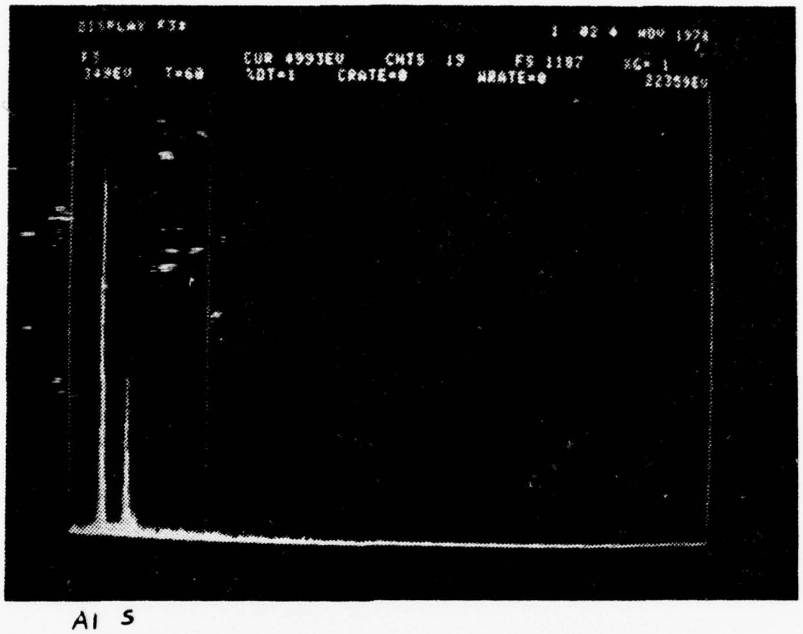

Figure 67

PGT-1000 X-ray spectrum of corrosion product on anode specimen 2DA1 after 2 day static exposure

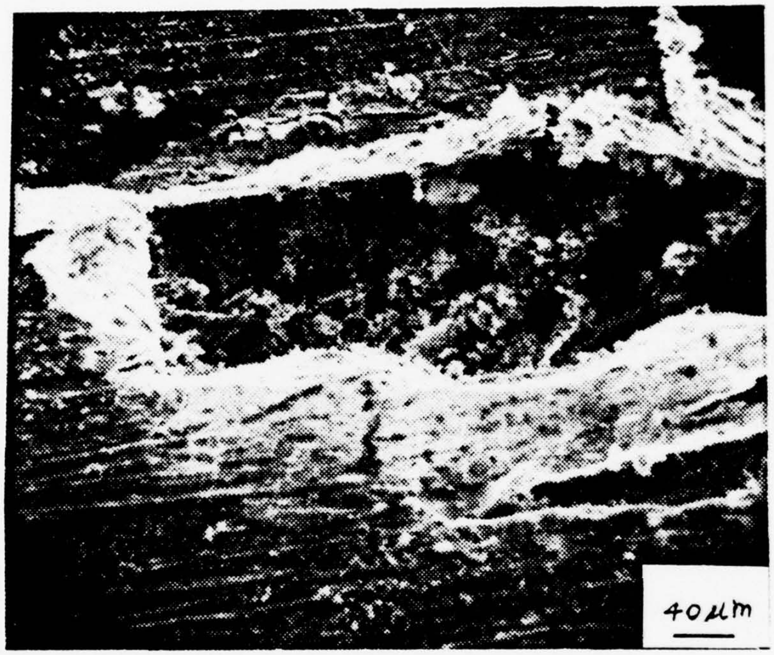

Figure 68

Aluminum anode specimen after 2 day static exposure showing pit, 225X (2DA1)

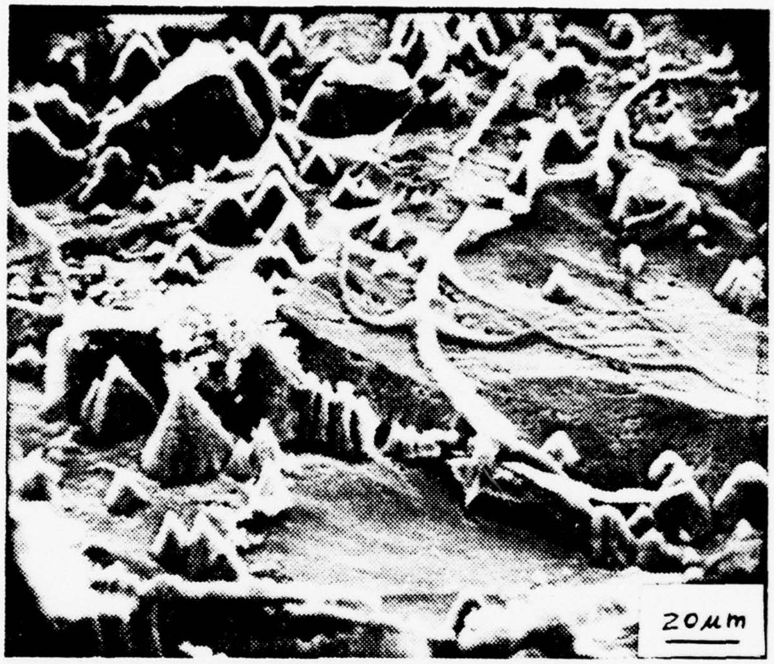

Figure 69

Aluminum anode specimen after 1 day static exposure showing pit bottom, 530X (1DA1)

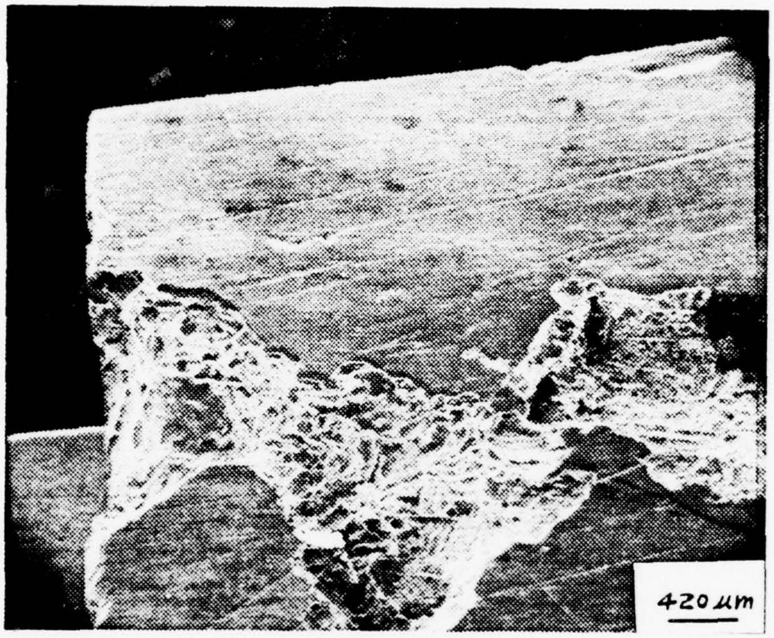

Figure 70

Aluminum anode specimen after 1 day static exposure and ultrasonic cleaning, 24X (1DA1)

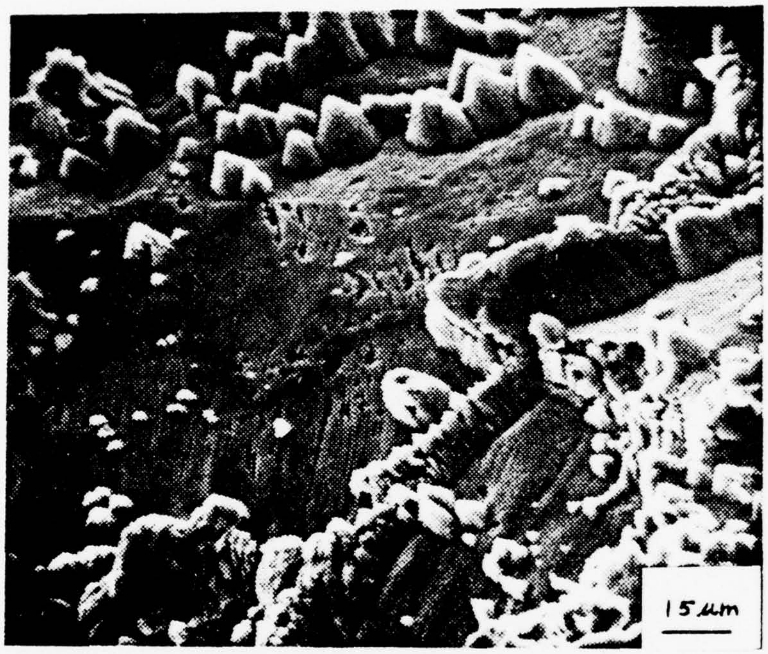

Figure 71

Aluminum anode specimen after 2 day static exposure showing pit surface, 660X (2DA1)

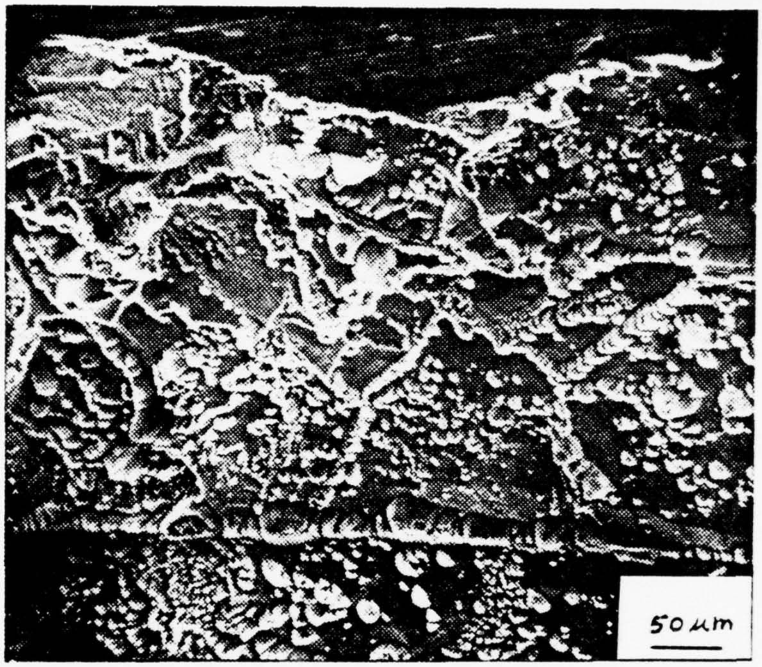

Figure 72

Aluminum anode specimen after 2 day static exposure showing pit side, 210X (2DA1)

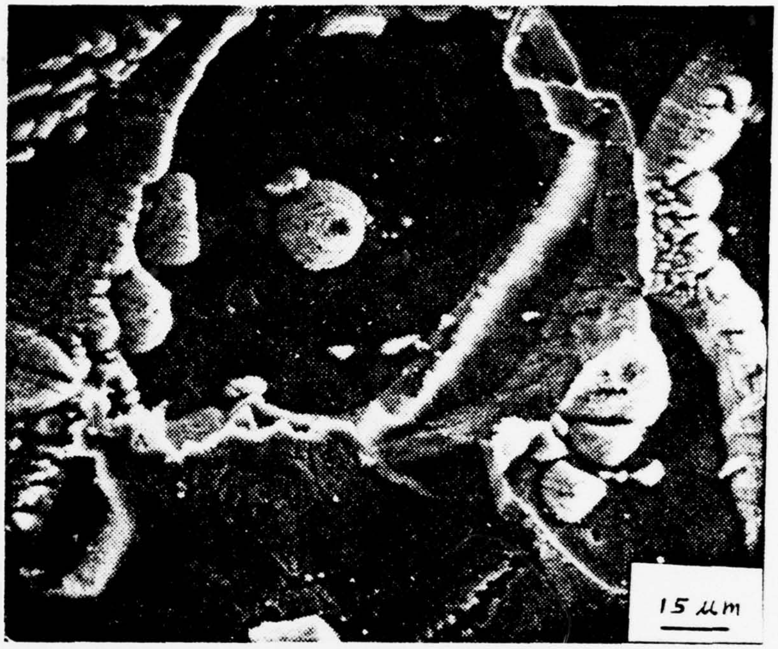

Figure 73

Aluminum anode specimen after 2 day static exposure showing pit surface, 650X (2DA1)

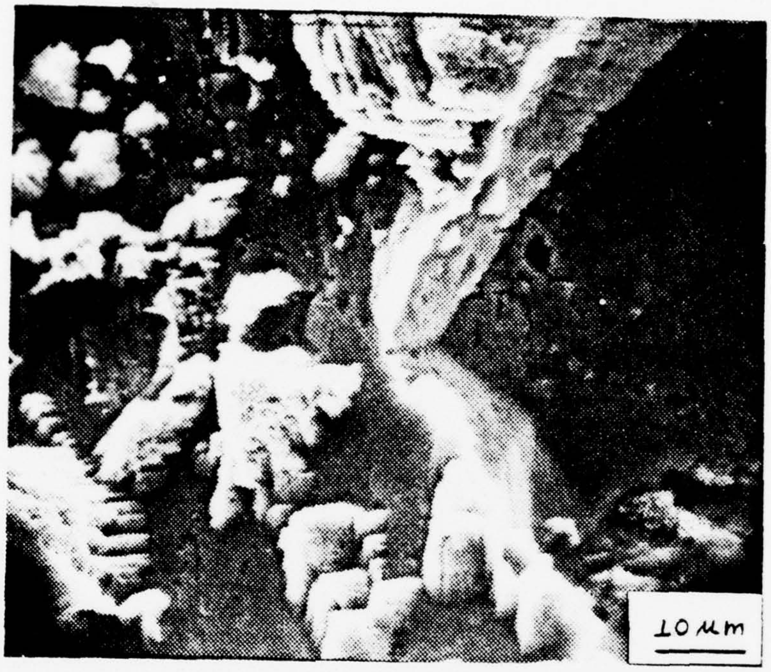

Figure 74

Aluminum anode specimen after 1 day static exposure showing pit surface, 1320X (1DA1)

and shows that these protrusions may not in fact be cone shaped but have somewhat octahedral shapes.

The corrosion pattern seen in these aluminum anode pits appears to be anti-intergranular in nature. The reasons for this pattern will now be hypothesized. It is reasoned that the grain boundaries have become cathodic to the grains due to a heterogeneous nucleation process at the grain boundaries. The slow cooling usually experienced by cast sacrificial anodes is appropriate for such a process. The large precipitate-free zones resulting within the grains are then anodic to the solute rich grain boundaries. The fact that aluminum is a face centered cubic (FCC) metal may explain why the precipitate rich grain boundaries tend to dissolve as they do. An FCC metal has the {111} crystallographic plane as its closest packed plane. It is hypothesized that the attack seen at the grain boundaries is proceeding somewhat parallel to the {111} planes, so that octahedra result and are seen as "hills" or "cones". Figure 75 is a PGT-1000 X-ray spectrum of an interior grain area of specimen 2DA1. Only the aluminum peak is in evidence. This suggests that no corrosion products are present, and the grain boundary precipitates are a phase of aluminum.

One further point that may be made is that the corrosive action along the sides of pits will continue to undercut the surface. This means that the passivating surface film may not be a significant factor in corrosion behavior of these anodes in a long term application. It also suggests that the corrosion rate will become more uniform with time, and parts

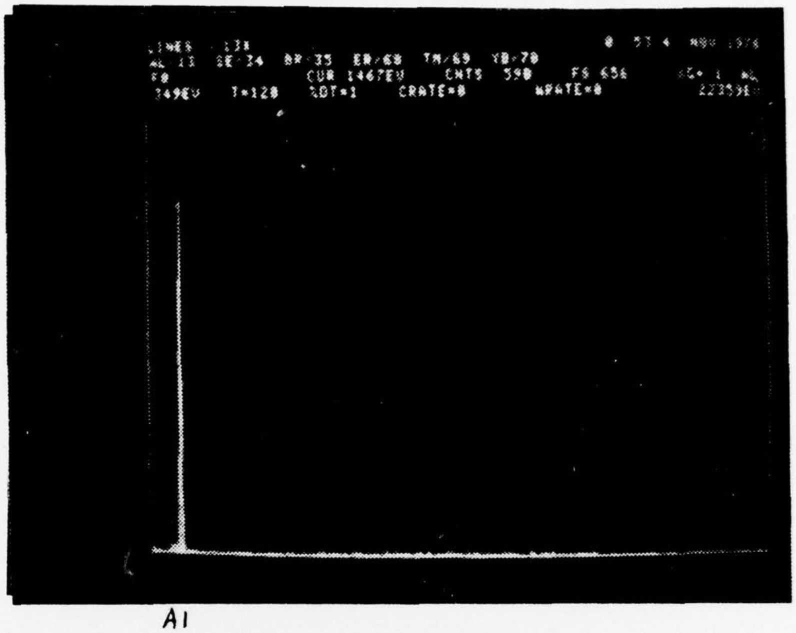

Figure 75

PGT-1000 X-ray spectrum of a grain sized area of anode specimen 2DA1 of the anode may not be isolated and therefore "lost" in service, as suspected by early Naval Research Laboratory investigators.

These microscopic studies of aluminum anodes are at an early stage. Much remains to be done in order to characterize adequately the behavior in cathodic protection situations.

IV. CONCLUSIONS

The following conclusions have been reached as a result of this work:

1. The corrosion product existing on a zinc sacrificial anode affects the subsequent corrosion behavior of that anode when subjected to finite relative velocity for a period of time.

2. Zinc sacrificial anodes undergo periods of reduced corrosion product adherence in quiescent electrolyte conditions.

3. There are distinct layers of corrosion product growth in quiescent electrolyte conditions. These layers manifest themselves as an outer layer of dense ZnO platelets, with larger platelets attached, and an intermediate mossy corrosion product layer in which the outer platelet layers are imbedded. The outer platelet layer growth rate decreases with time. The intermediate layer continues to grow at an unknown rate.

4. At natural galvanic current densities, corrosion products resulting from static exposures of less than 6 hours behave differently under dynamic exposure conditions than those resulting from static exposures of 12 hours or more. An incompletely defined platelet reforming or redeposition action takes place on dynamically exposed specimens for short static pre-exposure times. For longer static pre-exposures, no such action is evident, and ZnO platelet morphology remains

relatively unchanged. The reason for this behavior is thought to be the reduced diffusion of zinc ions through the thicker corrosion product layers.

5. Conditions of turbulent or laminar electrolyte flow produce different corrosion product behaviors. In the laminar flow regime, cracking of the dense outer platelet layer results in the forming of crust-like products on the corrosion product surface. It appears that previously existing platelets and precipitated compounds from the seawater are reformed or engulfed into this developing crust. The crust then cracks, revealing large areas of intermediate corrosion product below. This action is depassivating and allows electrolyte to penetrate more easily to the zinc surface. In the turbulent flow regime, the tendency for crust formation reduces, and cracked outer platelet layers are simply carried away by the turbulent electrolyte. This action is also considered depassivating. The greater availability of zinc ions in the laminar flow regime is considered to be the determining factor in crust formation.

6. The behavior of zinc anode corrosion products is depassivating in either turbulent or laminar flow regimes or in static exposure conditions.

7. Galvalum sacrificial aluminum anodes undergo widespread pitting attack in quiescent seawater conditions. The pitting attack is characterized by an anti-intergranular corrosion pattern which undercuts adjacent anode surface due to rapid recession of pit sides as well as bottoms.

8. At least in the early stages of exposure, large areas of Galvalum surface may be left unpitted in seawater, due to the presence of a natural passivating film.

V. RECOMMENDATIONS

The results of this study constitute a continuation of previous zinc corrosion product research, particularly in the areas of zinc sacrificial anode passivation tendencies, and a preliminary investigation into aluminum sacrificial anode behavior. Future research in these areas should concentrate on the following points.

1. It would be interesting to carry out further investigation of zinc sacrificial anode behavior at (higher) velocities which more closely simulate shipboard conditions. This might be accomplished through the use of a variable-flow chamber. The present work was limited to a velocity of approximately 10 fps (3.05 m/s).

2. Considerably more investigation is also needed on aluminum sacrificial anode corrosion behavior. Particularly, the effects of corrosion product morphology on anode performance, suitability of various commercial anodes to Navy applications, and further characterization of pitting corrosion mechanisms and behavior should be pursued.

TABLE I

CHEMICAL ANALYSIS OF ZINC SPECIMENS*

Metal	% Composition
Cadmium	0.0050
Iron	0.0030
Lead	0.0010
Aluminum	0.1200
Silicon	0.0010
Copper	0.0002
Zinc	Remainder

* Spectrographic analysis by Metallurgical Labs, Inc., San Francisco, California.

TABLE II

MILITARY SPECIFICATION: MIL-A-18001H
CHEMICAL COMPOSITION REQUIREMENTS, ZINC ANODES

Metal		% Composition
Cadmium	(range)	0.025-0.15
Iron	(maximum)	0.005
Lead	(maximum)	0.006
Aluminum	(range)	0.10-0.50
Silicon	(maximum)	0.125
Copper	(maximum)	0.005
Zinc		Remainder

TABLE III

CHEMICAL ANALYSIS OF ALUMINUM SPECIMENS*

Metal	% Composition
Iron	0.0800
Copper	0.0020
Zinc	0.6000
Silicon	0.0500
Magnesium	0.0100
Titanium	0.0100
Aluminum	Remainder

---

* Spectrographic analysis by Metallurgical Labs, Inc., San Francisco, California.

TABLE IV

SPECIMEN EXPOSURE COMPILATION

Zinc Anode Specimens

Specimen	Current Density mA/in^2	mA/cm^2	Dynamic Exposure Time Minutes	Disk rpm
.5HZ1	5	0.775	30	100
.5HZ2	5	0.775	60	100
1HZ1	5	0.775	10	100
1HZ2	5	0.775	30	100
1HZ3	5	0.775	60	100
2HZ1	5	0.775	30	100
2HZ2	5	0.775	30	150
2HZ3	5	0.775	30	200
3HZ1	0	0	30	100
3HZ2	0	0	30	150
3HZ3	0	0	30	200
6HZ1	5	0.775	30	150
6HZ2	0	0	30	150
6HZ3	5	0.775	60	150
6HZ4	0	0	60	150
12HZ1	5	0.775	60	150
12HZ2	5	0.775	120	150
12HZ3	6	0.775	180	150
24HZ1	not subjected to dynamic exposure			
24HZ2	" " " " "			
24HZ3	" " " " "			
36HZ1	5	0.775	120	100
36HZ2	5	0.775	120	150
36HZ3	5	0.775	120	200
2DZ1	5	0.775	180	100
2DZ2	5	0.775	180	50
2DZ3	15	2.325	180	100
3DZ1	not subjected to dynamic exposure			

TABLE IV (Continued)

Zinc Anode Specimens

Specimen	Current Density mA/in^2	mA/cm^2	Dynamic Exposure Time Minutes	Disk rpm
3DZ2	5	0.775	180	150
3DZ3	15	2.325	180	150
4DZ1	not subjected to dynamic exposure			
4DZ2	" " " " "			
4DZ3	" " " " "			
8DZ1	" " " " "			
8DZ2	" " " " "			
8DZ3	" " " " "			

Aluminum Anode Specimens

Specimen	Static Exposure Time - Hours
1HA1	1
6HA1	6
12HA1	12
1DA1	24
2DA1	48

APPENDIX A

PREPARATION OF ARTIFICIAL SEAWATER

Synthetic standard seawater required during experimentation was prepared using the formula and procedure developed by Kester, et al [23]. A concentrated stock solution was initially produced for ease in handling prior to use.

The following amounts of gravimetric and volumetric salts, combined with enough distilled water for a total weight of 1 kilogram, were used per kilogram of synthetic seawater solution.

A. Gravimetric Salts

Salt	g/kg of solution
$NaCl$	23.926
Na_2SO_4	4.008
KCI	0.677
$NaHCO_3$	0.196
KBr	0.098
H_3BO_3	0.026
NaF	0.003

B. Volumetric Salts

Salt	Conc M/L	ml/kg of solution
$MgCl_2 \cdot 6H_2O$	1.000	53.27
$CaCl_2 \cdot 2H_2O$	1.000	10.33
$SrCl_2 \cdot 6H_2O$	0.100	0.90

C. Distilled water to bring total weight to 1 kilogram

LIST OF REFERENCES

1. Uhlig, H. H., Corrosion and Corrosion Control, John Wiley & Sons, Inc., p. 20-214, 1971.

2. Benedict, R. L., "Anode Design for Shipboard Cathodic Protection," Materials Protection, v. 4, No. 12, p. 36-38, December 1965.

3. Fontana, M., Greene N., Corrosion Engineering, McGraw-Hill Book Company, p. 37-49; 60-91; 1967.

4. Birnbaum, L., Taylor, B., Strasburg, W., "Cathodic Protection," Naval Engineers Journal, April 1971, p. 13-24, April 1971.

5. Davy, H., "On the Corrosion of Copper Sheathing on Ships by Seawater, and a Method of Preventing This Effect; and in Their Application to Ships of War and Other Ships," Phil. Trans. Roy. Soc. (London), 1824; Corrosion, v. 3, p. 295, 1947.

6. Francis, R. C. and Cook, F. E., "Economics of Cathodic Protection for U.S. Navy Ships," Materials Protection, v. 1, No. 2, p. 18-20; 22-23; 1962.

7. Teel, R. B. and Anderson, D. B., "The Effect of Iron in Galvanic Zinc Anodes in Sea Water," Corrosion, v. 12, p. 53-59, 1956.

8. Southin, R. T., "Some Observations on the Microstructure of Zinc Alloy Anodes," J. Inst. Metals, v. 93, p. 428-431, 1964-65.

9. Reichard, E. C., and Lennox, T. J., "Shipboard Evaluation of Zinc Galvanic Anodes Showing the Effect of Iron, Aluminum, and Cadmium on Anode Performance," Corrosion, v. 13, p. 410-416, 1957.

10. Waldron, L. J., and Peterson, M. H., "Effect of Iron, Aluminum, and Cadmium Additions on the Performance of Zinc Anodes in Sea Water," Corrosion, v. 16, p. 375-379, 1960.

11. Military Specification MIL-A-18001H, Anodes, Corrosion Prevention, Zinc; Slab, Disc, and Rod Shaped, 28 June 1968.

12. Kurr, G. W., "Sacrificial Anode Applications in Ships," Materials Protection, v. 8, No. 11, p. 19-23, November 1969.

13. Lennox, T. J., "Electrochemical Properties of Magnesium, Zinc, and Aluminum Galvanic Anodes in Sea Water," *Proceedings of the 3rd Int. Cong. on Marine Corrosion and Fouling*, NACE, p. 176-190, 1972.

14. Haney, E. G., and Kurr, G. W., *Seawater Tests of Aluminum Alloy Anodes Containing Zinc, Indium and Cadmium*, paper presented at National Association of Corrosion Engineers Northeast Regional Meeting, Hartford, Connecticut, 7-9 October 1975.

15. Private communication with T. J. Lennox, Naval Research Laboratory, July 1976.

16. Money, N. T., "Deep Ocean Corrosion-Simulation Facilities vs. In-Situ Research," *Materials Protection and Performance*, v. 12, No. 1, p. 10-13, January 1973.

17. Mor, E. D. and Beccaria, A. M., "Effect of Temperature on the Corrodibility of Copper and Zinc in Synthetic Seawater," *Corrosion*, v. 31, No. 8, p. 275-279, August 1975.

18. Bornholdt, R. A., and Perkins, A. J., "SEM Examinations of Corrosion Product Morphology for Anodically Polarized Zinc," *Mettalography*, v. 8, p. 39-47, 1975.

19. Todd, J. M., and Perkins, A. J., "Corrosion of Zinc Anodes in Seawater," *Naval Engineers Journal*, v. 88, No. 4, p. 65-72, August 1976.

20. Todd, J. M., and Perkins, A. J., "Nucleation and Growth of Anodic Electrocrystallization Products on Zinc in Saltwater Solutions," *Corrosion*, (in press, 1976).

21. Todd, J. M., *Nucleation and Growth of Anodic Electrocrystallized Products on Ship Hull Zinc in Salt Water Solutions*, MSME-Mechanical Engineer Thesis, Naval Postgraduate School, December 1975.

22. Luebke, W. H., *A Scanning Electron Microscope Study of the Effects of Anode Velocity and Current Density on the Corrosion of Ship Hull Zinc in Synthetic Seawater*, MSME Thesis, Naval Postgraduate School, June 1976.

23. Kester, D. R., Duedall, I. W., Conners, D. N., and Pytkowicz, R. M., "Preparation of Artificial Seawater," *Limnology and Oceanography*, v. 12, p. 176-178, December 1967.

24. Simmons, J. A., Coriell, S. R. and Ogburn, F., "Calculation of Currents of Local Galvanic Cells," *Journal of the Electrochemical Society*, v. 114, No. 8, p. 782-787, August 1967.

25. Champion, F. A., Corrosion Testing Procedures, John Wiley & Sons, Inc., p. 282-283, 1965.

26. Galvele, J. R., "Transport Processes and the Mechanism of Pitting of Metals," Journal of the Electrochemical Society, v. 123, No. 4, p. 464-474, April 1976.

27. White, R., Mohr, C. and Newman,J., "The Fluid Motion Due to a Rotating Disk," Journal of the Electrochemical Society, v. 123, No. 3, March 1976.

28. Riddiford, A. C., "The Rotating Disk System," Advances in Electrochemistry and Electrochemical Engineering, v. 4, John Wiley & Sons, Inc., p. 47-116, 1966.

29. Farmer, E. D., and Webb, A. H., "Zinc Passivation and the Effect of Mass Transfer in Flowing Electrolyte," Journal of Applied Electrochemistry, v. 2, p. 123-139, 1972.

30. Devanathan, M. A., and Guruswamy, V., "Investigation of Mass Transfer in Flowing Electrolytes, II. Turbulent Flow Conditions," Electrokhimiya, v. 7, No. 12, p. 1818-1825, December 1971.

31. Böhni, H. and Uhlig, H. H., "Environmental Factors Affecting the Critical Pitting Potential of Aluminum," Journal of the Electrochemical Society, v. 116, No. 7, p. 906-910, July 1969.

INITIAL DISTRIBUTION LIST

		No. Copies
1.	Defense Documentation Center Cameron Station Alexandria, Virginia 22314	2
2.	Library, Code 0212 Naval Postgraduate School Monterey, California 93940	2
3.	Department Chairman, Code 69 Department of Mechanical Engineering Naval Postgraduate School Monterey, California 93940	2
4.	Professor A. J. Perkins, Code 69 Department of Mechanical Engineering Naval Postgraduate School Monterey, California 93940	5
5.	LCDR Peter W. Wright Naval Reactors Representative Office Energy Research and Development Admin. Post Office Box 2053 Vallejo, California 94592	2
6.	Mr. Kenneth J. Graham, Code 61Kg Department of Physics and Chemistry Naval Postgraduate School Monterey, California 93940	1